processes

MDPI

Review

Advances in Polyaniline-Based Composites for Room-Temperature Chemiresistor Gas Sensors

Clinton M. Masemola [1,2]**, Nosipho Moloto** [1]**, Zikhona Tetana** [3]**, Linda Z. Linganiso** [4]**, Tshwafo E. Motaung** [5] **and Ella C. Linganiso-Dziike** [1,2,5,*]

1   Molecular Sciences Institute, School of Chemistry, University of the Witwatersrand, Private Bag 3, Johannesburg 2050, South Africa
2   DSI/NRF Centre of Excellence in Strong Materials, University of the Witwatersrand, Braamfontein 2050, South Africa
3   Institute for Nanotechnology and Water Sustainability, College of Science, Engineering and Technology, University of South Africa, Florida Campus, Johannesburg 1709, South Africa
4   Institute for Catalysis & Energy Solutions (ICES), University of South Africa, Florida Campus, Johannesburg 1709, South Africa
5   Department of Chemistry, Sefako Makgatho Health Science University, P.O. Box 94, Medunsa, Ga-Rankuwa, Pretoria 0204, South Africa
*   Correspondence: cebisa.linganiso@wits.ac.za or linganisoella@gmail.com; Tel.: +27-11-717-1339

Abstract: The increasing rate of environmental pollution and the emergence of new infectious diseases have drawn much attention toward the area of gas sensors for air quality monitoring and early-stage disease diagnosis, respectively. Polyaniline (PANI) has become one of the extensively studied polymers in the area of chemical sensing due to its good conductivity and sensitivity at room temperature. The development of room-temperature gas sensors represents a significant leap forward in air quality monitoring by conserving energy and enhancing the feasibility of the commercial development of sensing technologies. New research shines a light on the advantages of using PANI with materials such as semiconductor metal chalcogenides, metal oxides, metal nanoparticles, and graphitic carbon materials to form composites that can sense chemicals selectively at room temperature. This review focuses on the advancements in PANI-based gas sensors, exploring the materials, mechanisms, and applications that make these sensors a promising solution for modern air quality monitoring challenges. By examining the latest research and innovations, we aim to highlight this critical technology's potential and future directions, instilling hope and optimism in safeguarding public health and the environment.

Keywords: polyaniline; chemical sensors; nanomaterial composites; room-temperature sensors; semiconductors; enhanced selectivity; enhanced sensor performance

1. Introduction

The Industrial Revolution has brought notable advantages to humankind's overall living and working conditions, such as increased production systems resulting in economic growth, access to information, improved living conditions, urbanization, innovative transportation, and overall machinery. This has come with notable disadvantages; rapid industrialization and urbanization have significantly increased the release of harmful products into the environment, negatively affecting the environment and human health. Thus, today we face the issue of global warming, which is mainly caused by carbon-emitting industrial processes and transportation corresponding to increased energy demands. The interest in gas sensing is meant to address air quality monitoring (indoor and outdoor) as

well as human health. These concepts feature in the United Nations (UN)'s Sustainable Development Goals (SDGs). According to the World Health Organization (WHO), 99% of the global population breathes air that exceeds WHO guideline limits of pollutants [1]. Many industrial processes produce pollutants such as toluene, benzene, particulate matter (PM_X), ammonia (NH_3), carbon monoxide (CO), hydrogen sulfide (H_2S), nitrogen dioxide (NO_2), sulfur dioxide (SO_2), and carbon dioxide (CO_2), which directly or indirectly contribute to global warming and human health deterioration.

With regard to human health, there are short-term and long-term effects of exposure to pollutants in the air. Short-term exposure often leads to irritation of the eyes, nose, and throat along with symptoms like headache, dizziness, and allergic reactions [2]. These effects are usually temporary and may disappear once exposure ceases. However, long-term exposure is severe, potentially causing chronic respiratory issues, harm to vital organs like the liver and kidneys, and an elevated risk of cancer, as depicted in Figure 1 [2].
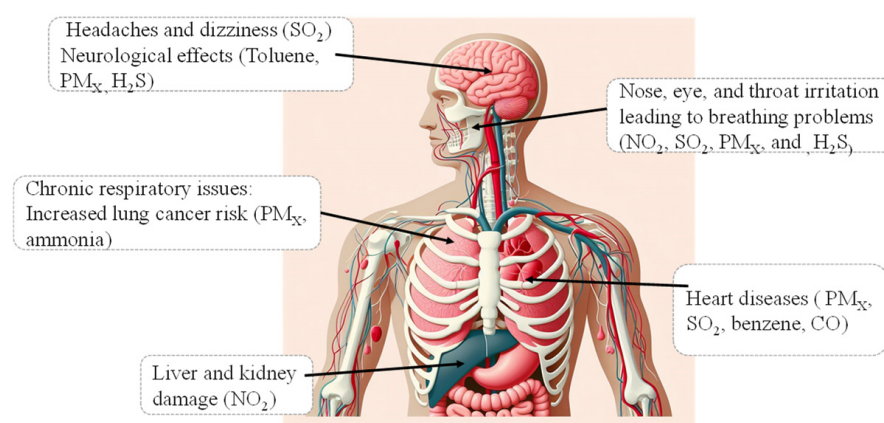
Figure 1. A schematic showing symptoms caused by exposure to toxic substances in air. Image created by use of artificial intelligence (AI).

Given these risks, addressing air pollution is paramount. The Occupational Safety and Health Administration (OSHA) has passed regulations to limit exposure to these hazardous substances that are recognized worldwide, as outlined in Table 1 [3]. The effective management of air quality requires advanced technological solutions for monitoring and control. Among these, gas sensors have emerged as vital tools. These devices detect and measure specific gases in the atmosphere, providing essential data for air quality monitoring [4]. Polyaniline (PANI) nanocomposites have become prominent materials in the development of room-temperature gas sensors owing to their remarkable properties and versatility. When combined with components such as hollow carbon spheres or metal oxides, these nanocomposites exhibit excellent electrical conductivity, thermal stability, and heightened sensitivity across a broad spectrum of gases [5,6]. A key benefit of PANI-based sensors is their efficient operation at room temperature, which removes the necessity for external heating elements, thereby reducing energy consumption and simplifying the design process. Additionally, these nanocomposites can be synthesized easily through chemical oxidation methods, making them both cost-effective and scalable for industrial applications. Their high surface areas and porous structures promote enhanced gas adsorption, resulting in swift response and recovery times [6]. Consequently, they prove to be highly effective in detecting various gases including NH_3, CO_2, and volatile organic compounds (VOCs) with outstanding selectivity and sensitivity [6]. Overall, the incorporation of PANI nanocomposites into gas sensors represents a promising pathway for the development of efficient, low-cost, and environmentally sustainable sensing technologies.

Table 1. OSHA permissible exposure limits for various gases and particulate matter [3].

Pollutants	Short-Term Exposure (STEL)	Long-Term Exposure (TWA)
Toluene	300 ppm	200 ppm
Benzene	5 ppm	1 ppm
Particulate Matter	-	10 mg/m^3
Ammonia	35 ppm	25 ppm
Carbon Monoxide	400 ppm	50 ppm
Hydrogen Sulfide	15 ppm	10 ppm
Nitrogen Dioxide	5 ppm	5 ppm
Sulfur Dioxide	5 ppm	2 ppm
Carbon Dioxide	-	5000 ppm

2. Different Gas Sensor Technologies

Gas sensors have been used since the early 19th century. To date, various types of sensors have been used such as catalytic gas sensors, electrochemical gas sensors, thermal conductivity gas sensors, optical gas sensors, non-dispersive infrared (NDIR) gas sensors, semiconductor gas sensors, surface acoustic wave (SAW) sensors, gas chromatograph analyzers, film bulk acoustic resonators (FBARs), photoionization detector gas sensors (PIDs), and chemiresistor gas sensors. Some of these types of gas sensors are summarized below.

2.1. Catalytic Gas Sensors

A catalytic gas sensor is also known as a pellistor. The sensor, designed with safety in mind, consists of two beads: a catalytic bead and a reference bead. Both beads contain a platinum wire coil embedded in a ceramic material, as illustrated in Figure 2. The catalytic bead is sensitive to flammable gases, while the reference bead (inert and non-reactive) provides a constant baseline signal without reacting to gases, ensuring accurate detection of flammable gases for safety [7]. When combustible gases (such as methane, propane, and hydrogen) react with oxygen, they produce heat in an exothermic reaction on the catalyst's surface within the detector, known as catalytic combustion. This process allows ignition at lower temperatures, which is crucial for detecting potentially hazardous and explosive gases [7]. The sensor uses a Wheatstone Bridge-type circuit to convert the change in electrical resistance caused by temperature increases within the detector coil due to gas oxidation into an electrical signal. This signal directly reflects the gas concentration being measured. The operating principle of a catalytic combustion-based gas sensor involves a temperature change resulting from the exothermic reaction of the detected gas on the catalyst surface. It offers robust and easy operation, simple installation, low replacement cost, and suitability for challenging environments like dusty, dirty, and high-temperature settings [7]. However, limitations such as catalyst contamination, oxygen requirement for detection, and considerations for prolonged use should be noted. Also, the ideal temperature range for detecting hydrocarbons is 900–1000 °C, but platinum evaporates, and its resistance increases at these temperatures [7]. To address this, Kalinin et al. developed a high-performance microheater-based catalytic hydrogen sensor on a porous substrate made of anodic aluminum oxide (AAO) coated with a platinum (Pt) layer (Pt/AAO) [8]. The sensors achieved a hydrogen sensitivity of 76 mV/vol%, with a fast response time of 0.4 s and long-term stability, showing less than 4% deviation over 14 days of continuous operation. Operating at an active zone temperature of 500 °C, the sensors maintained low power consumption of 3.2 mW in pulsed power supply mode [8]. The detection limit was estimated to be 12 ppm. The study utilized a pulsed power supply mode to reduce the operating temperature, enhancing the sensors' efficiency [8].
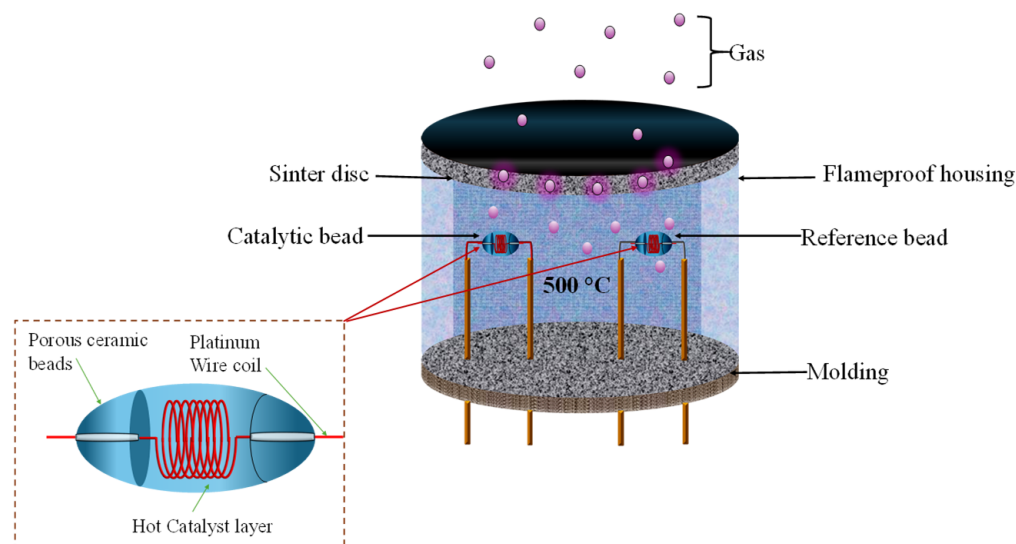
Figure 2. Schematic representation of a catalytic bead sensor.

2.2. Thermal Conductivity Gas Sensors

The operating principle of thermal gas sensors, comparable to catalytic sensors, shows significant potential for future advancements. These sensors feature two microheaters: one exposed to the target gas (the detector) and the other enclosed in an air-filled chamber (the compensator) (see Figure 3) [9]. They function within a circuit configuration similar to that of catalytic sensors, enabling their use in the same Wheatstone Bridge circuits due to their comparable electrical characteristics. When the detector microheater encounters a gas with a thermal conductivity significantly different from that of air, its heat loss rate changes, which in turn alters its resistance [9]. This variation is subsequently compared with the resistance values of the compensator microheater for analysis. These sensors are particularly effective for detecting low-molecular-weight gases with higher thermal conductivities than air, as these gases produce the highest sensor response. However, gases such as CO, nitrogen, and oxygen have thermal conductivities similar to air, making them difficult to measure effectively [9]. Additionally, the sensitivity of these sensors may vary with gas temperature. Thermal conductivity sensors are frequently employed in environments such as coal mines and natural gas facilities, where methane concentrations can surpass 50% by volume in coal seams. They are also ideal for monitoring light gases like helium and hydrogen. These sensors offer numerous advantages: they are cost-effective, consume less power, do not rely on adsorption or catalysts, have a longer operational lifespan, and are compact [10]. However, they also face challenges such as cross-sensitivity to ambient humidity and temperature, low sensitivity, and poor selectivity. Overcoming these challenges is a key focus for future advancements in sensing technology, which could potentially revolutionize the microelectromechanical systems' (MEMS') gas sensing market by offering cheaper, smaller, and more energy-efficient solutions, a prospect that is highly valued in modern applications [10]. Gardner and coworkers introduced an innovative MEMS technology specifically for detecting CO_2 levels, utilizing the principle of differential thermal conductivity [11]. The sensor was designed with holes in a thin-film dielectric membrane that helped create an uneven temperature distribution, which was generated by a tungsten resistor located at the center. This unique setup allowed for varied gas interaction magnitudes across the sensor, a finding that was validated by numerical modeling [11]. Measurements of CO_2 concentration were obtained through differential readings from four resistors positioned around the sensor. The optimal combination of resistors provided a sensitivity of 0.05 mV per percent of CO_2 [11]. By utilizing separate heating and sensing

elements, the noise was significantly reduced, leading to a detection resolution of less than 100 ppm. This proof-of-concept device demonstrated potential for low-cost, low-power, high-sensitivity, scalable gas detection [11].
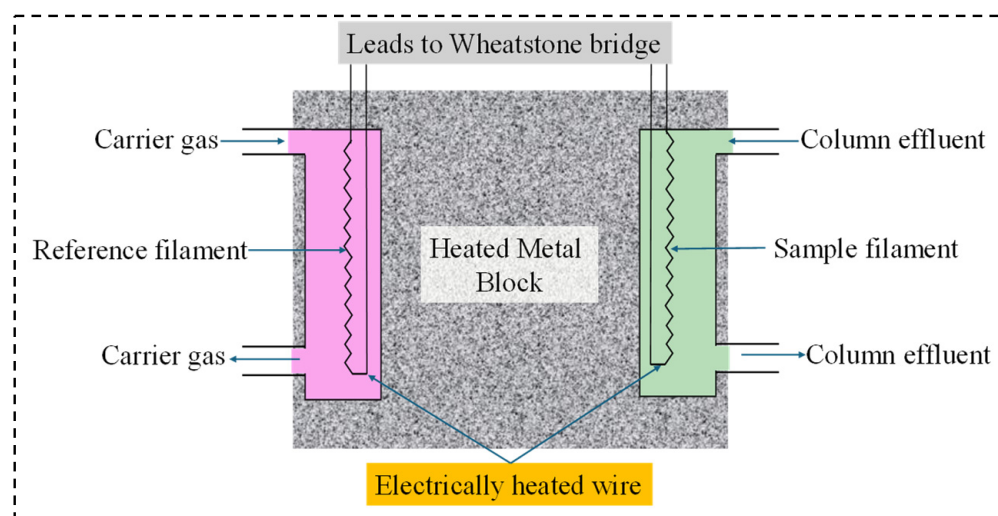
Figure 3. Schematic representation of a thermal conductivity gas sensor.

2.3. Electrochemical Gas Sensors

Electrochemical sensors work by interacting with the target gas and an electrolyte within the sensor. When the target gas contacts the electrode surface, it initiates a chemical reaction, creating an electric signal proportional to the gas concentration. This principle enables the accurate measurement and detection of various gases in different applications. The setup of the electrochemical sensor involves a system consisting of a counter electrode, a reference electrode, and a working electrode, all of which are separated by a thin layer of an electrolyte [12] (see Figure 4). Various electrochemical methods such as voltammetry, amperometry, potentiometry, impedimetry, and conductometry are employed to generate digital signals, which are later analyzed to determine the concentration of analytes [12]. Potentiometry quantifies the analyte concentration by measuring the potential difference between working and reference electrodes without the need for current flow. This open-circuit voltage varies with the analyte concentration, providing the analytical signal. Impedimetry assesses electrical impedance, including parameters like charge transfer resistance, which correlates with analyte activity [12]. Voltammetry is a technique used to measure the analyte concentration by observing how it responds to changes in potential during a redox reaction. The potentiostat is used in various electrochemical techniques such as linear or cyclic voltammetry and square wave voltammetry [12]. It sets the voltage difference between the electrodes and interprets the resulting current as the analytical signal. Amperometry is a time-dependent method that tracks variations in current response under constant potential, yielding in-depth insights into analyte behavior. These combined techniques facilitate accurate and adaptable electrochemical analysis, each tailored to specific measurement requirements and types of analytes [12]. In a recent study by Hosseini and co-workers, a borophene-based electrochemoresistance (ECR) sensor was developed [13]. This sensor combined electrochemical and chemiresistive gas sensing, demonstrating a high sensitivity that was 10 times greater than conventional electrochemical sensors and 4 times greater than chemiresistive sensors. It excelled in detecting hydrogen sulfide (H_2S) gas, with a sensitivity of approximately 2.11 μA/ppm and a fast response time of 6–8 s [13]. The sensor also maintained good stability at 35% humidity over three months, making it a promising candidate for future gas-sensing applications. Electrochemical sensors offer advantages such as being customizable for specific gases or vapors in the parts per million

(ppm) range, differences in Faradaic and non-Faradaic currents leading to low theoretical detection limits, linear response for simplified calibration and precise measurement, and excellent repeatability and accuracy once calibrated. However, they depend on oxygen for accurate detection and may have a limited lifespan, requiring periodic maintenance.
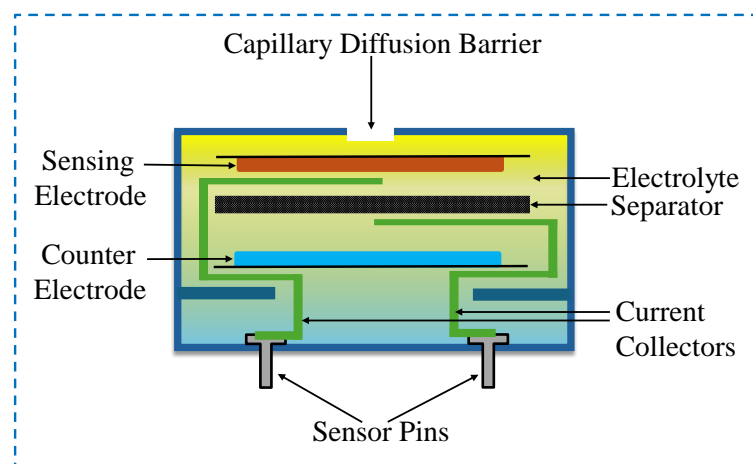
Figure 4. Schematic representation of an electrochemical sensor.

2.4. Optical Gas Sensors

Fiberoptic VOC gas sensors have emerged as an innovative technology for detecting VOCs. Originating in the late 1980s, compared with traditional methods, these sensors offer distinct advantages such as high sensitivity, selectivity, and the ability to operate remotely using optical fibers [14]. A typical fiberoptic gas-sensing system comprises essential components such as a gas chamber that contains the target gas for analysis, a light detector, a light source (laser or broadband), the fiberoptic gas-sensing probe, input and output fibers for transmitting light to and from the sensing probe, and a demodulator to process the modulated optical signals received from the probe (see Figure 5) [14]. The operating principle involves directing light from the source to the modulation area inside the fiberoptic sensing probe. When the gas chamber receives the target gas, it interacts with the light within the modulation zone, modulating the optical properties. These modulated signals travel through the optical fiber and reach the optical detector and demodulator, where the measured parameters are obtained [14]. Optical fiber gas sensors offer several advantages, including immunity to electromagnetic interference, remote sensing capabilities over long distances, multiplexing for cost-effective solutions, and a compact and lightweight design that easily integrates into existing systems [14]. However, these sensors also have drawbacks such as the relatively high initial setup costs, unfamiliarity among end users compared with traditional sensors, and their sensitivity to physical damage, necessitating careful handling and protection [14]. Liu et al. conducted a detailed study to develop a new fiberoptic sensor for detecting ethanol gas using a special coating made from $ZnSnO_3$ nanoparticles and TiO_2 [15]. The sensor operated by utilizing ultraviolet (UV) light, which significantly boosted its sensitivity. It demonstrated a high sensitivity of 3.85 pm/ppm for ethanol concentrations ranging from 0 to 250 ppm, which was approximately 6.6 times more sensitive than similar sensors that did not use UV light [15]. The sensor also proved to be stable, had a rapid response time of about 20 s, and was highly selective toward ethanol gas. This research underscored the importance of UV light in enhancing gas sensor performance and marked the first use of $ZnSnO_3/TiO_2$ composite materials in fiberoptic sensors [15].
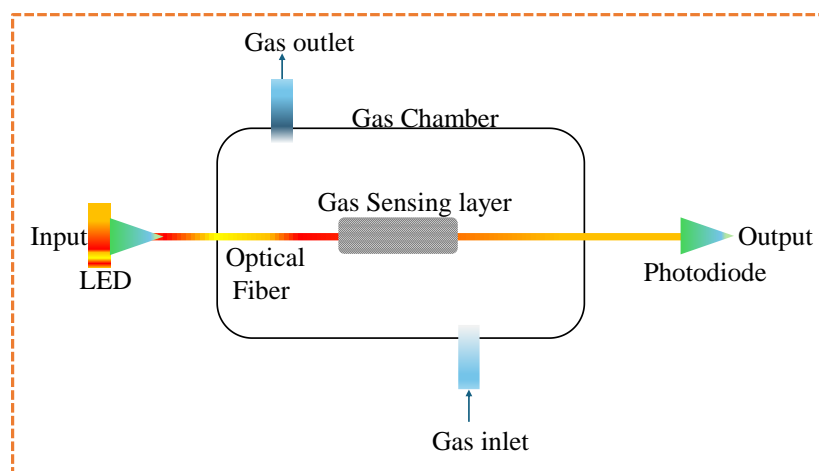
Figure 5. Schematic representation of an optical gas sensor.

2.5. Non-Dispersive Infrared (NDIR) Sensor

The operating principle of the NDIR gas detection method utilizes gas molecular absorption spectroscopy, in which gases absorb specific infrared radiation, resulting in thermal effect changes that are converted into electrical signals for detecting gas concentration [16]. NDIR sensors can detect many different gases at the same time because of the unique way each gas absorbs infrared light. These sensors have an infrared light source, a space to hold the gas (gas chamber), and a detector (Figure 6) [16]. In the infrared (IR) band, gases exhibit a unique fingerprint characteristic. Each gas absorbs specific wavelengths when exposed to infrared radiation, resulting in thermal effects. Detectors then convert these thermal changes into electrical signals, allowing the precise measurement of gas concentrations [16]. This phenomenon is analogous to a human fingerprint, wherein each gas's absorption spectrum is distinct and indicative of its identity [16]. This method has a durable working life, low energy consumption, high sensitivity, and stability, which make it superior to other techniques like semiconductor or electrochemical sensors. However, it faces obstacles such as gases interfering with each other, humidity interference, and a weak signal-to-noise ratio due to gases having low infrared absorption [16].
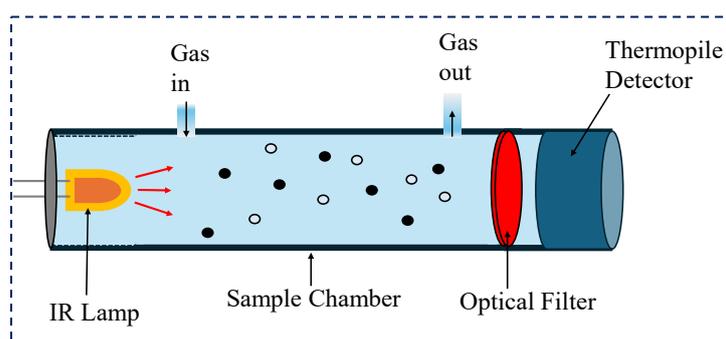
Figure 6. Schematic representation of a non-dispersive infrared gas sensor.

In a study by Yu et al., researchers developed a compact CO_2 detection system using non-dispersive infrared (NDIR) technology [17]. This sensor integrated an infrared light source and a dual-channel pyroelectric detector within a reflective gas chamber, allowing for a longer optical path and improved sensitivity in a small design [17]. The sensor demonstrated high accuracy, with a maximum detection error of less than 0.12% and a repeatability deviation of under 1.04% [17]. It also maintained stability during a 12 h test, with a maximum concentration drift of just 0.07%. These features made the sensor suitable for monitoring CO_2 safety in coal mines.

2.6. Semiconductor Gas Sensor

Semiconductor gas sensors operate by detecting changes in a semiconductor material's resistance when exposed to target analyte gases. Typically, these sensors comprise a sensing element made from metal oxides (e.g., tin dioxide (SnO_2)) integrated onto a substrate with electrodes and a heater, as shown in Figure 7. The metal oxide layer is porous, to increase the surface area for gas interaction, and when gases adsorb onto the metal oxide surface, the sensor's electrical conductivity changes, altering its resistance. The important components of these sensors include the sensing layer, heater coil, electrodes, tubular ceramic substrate, and protective case [18]. The heater plays a crucial role by increasing the temperature of the sensing element. By maintaining temperatures above 200 °C, the heater accelerates the reversible gas adsorption process rate. This elevated temperature enhances gas interaction with the oxide surface, leading to more rapid changes in electrical resistance [18]. Semiconductor sensors have advantages, such as a simple and cost-effective design, high sensitivity to a range of gases, and broad applicability in safety and security systems. However, they also have limitations, including a limited linear measurement range and susceptibility to interference from other gases and ambient temperature fluctuations [18].
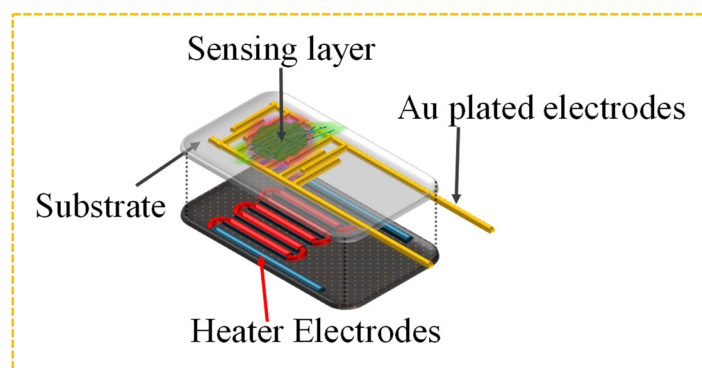
Figure 7. Schematic representation of a semiconductor gas sensor.

In the study by Yan et al., a high-performance room-temperature NO_2 gas sensor was developed using MoS_2/MoO_3 nanoparticle heterojunctions [19]. The sensor, created by oxidizing MoS_2 nanosheets in an H_2O_2 solution, exhibited a significant response of 18.9% to 1 ppm NO_2, which is 9 times higher than that of the MoS_2 sensor [19]. At a low NO_2 concentration of 50 ppb, the sensor achieved a response of 6.9%. The sensor also demonstrated good repeatability and excellent selectivity, making it a promising candidate for NO_2 gas-sensing applications [19].

2.7. Surface Acoustic Wave (SAW) Sensor

SAW sensors operate based on the transmission of elastic waves along the surface of a piezoelectric material [20]. The alteration of wave properties such as velocity and attenuation due to the presence of gas molecules allows for the detection of gases. The key components of these sensors include a SAW chip with interdigital transducers for wave generation and detection as well as a sensing material to interact with the target gas (see Figure 8) [20]. This mechanism boasts the advantages of SAW sensors, including their low cost, high sensitivity, fast response, low power consumption, and compatibility with MEMS technologies. However, stability poses a critical challenge to their commercial applications, as it significantly impacts their long-term reliability and accuracy [20]. Previous research has predominantly concentrated on the development of new materials and designs to enhance sensitivity and selectivity, with comparatively less emphasis on addressing stability issues. However, challenges exist in terms of selectivity, as certain materials may respond to

multiple gases. Environmental factors like temperature and humidity can also impact sensor performance [20,21].
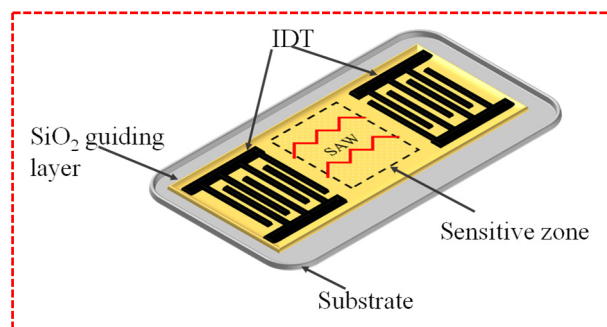
Figure 8. Schematic representation of a SAW sensor.

In a study by Buiculescu et al., a highly sensitive graphene-based surface acoustic wave (SAW) sensor was developed to detect nitrogen dioxide (NO_2) at room temperature [22]. This innovative sensor employed bilayer graphene (Bl-Gr) and sulfur-doped graphene (S-Gr) integrated with lithium tantalate ($LiTaO_3$) SAW devices. The Bl-Gr SAW sensor achieved a sensitivity of $0.29°/ppm$, with a limit of detection (LOD) of 0.068 ppm [22]. In comparison, the S-Gr SAW sensor displayed a sensitivity of $0.19°/ppm$ and an LOD of 0.140 ppm. Notably, the Bl-Gr SAW sensor demonstrated superior selectivity and performance in the presence of interfering gases and under varying humidity conditions, highlighting its potential as a promising candidate for NO_2 gas-sensing applications [22].

2.8. Thin-Film Bulk Acoustic Resonator (FBAR)

A Thin-Film Bulk Acoustic Resonator (FBAR) is a device composed of a piezoelectric material sandwiched between two conductive electrodes, typically metallic, and acoustically isolated from the surrounding medium, illustrated in Figure 9 [23]. The basic structure includes a bottom electrode, a piezoelectric layer, and a top electrode, all deposited on a silicon substrate [23]. When an alternating current (AC) signal is applied to the piezoelectric material, it converts the electrical signal into a mechanical or acoustic wave that propagates longitudinally within the FBAR device. This wave is then reflected back from the bottom electrode, creating a resonance condition. The resonance frequency is highly sensitive to changes in mass loading on the resonator, making FBARs useful for micro-mass sensing applications [23]. FBARs offer several advantages, including high sensitivity to mass changes, compact size for easy integration into electronic devices, low power consumption, and operation at high frequencies, which is beneficial for precise measurements [23,24]. However, they also have disadvantages, such as complex and costly fabrication processes, sensitivity to temperature changes that can affect performance and accuracy, and limited choices of piezoelectric materials, which can restrict their design and application.
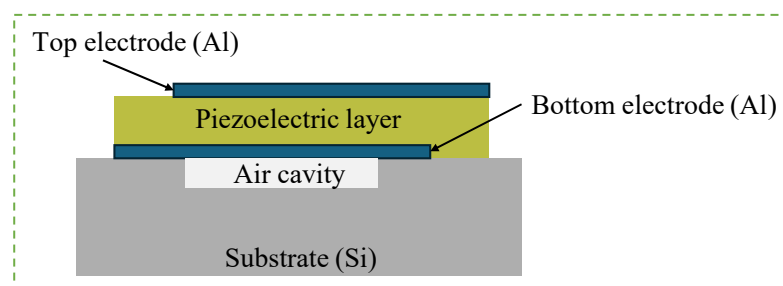
Figure 9. Schematic representation of an air gap FBAR gas sensor.

Gao et al. developed a high-performance virtual sensor array (VSA) utilizing a single-chip FBAR to detect and classify VOCs [25]. The FBAR, enhanced with a MIL-101(Cr) thin film, exhibited exceptional sensitivity and accuracy in VOC detection, calibrated through the Langmuir adsorption model. The sensor achieved a sensitivity of 85.45 Hz/ppm and a limit of detection (LOD) of 51 ppm for isopropanol [25]. The VSA's identification and classification capabilities were confirmed using statistical methods and machine learning algorithms, achieving 100% classification accuracy for pure VOCs and 94.6% for mixtures [25].

2.9. Photoionization Detectors (PIDs)

Photoionization detectors (PIDs) are sophisticated devices designed to detect VOCs and other gases. They operate by utilizing UV light to ionize gas molecules within an ionization chamber. The structure of a PID includes a UV lamp, an ionization chamber, and electrodes, as illustrated in Figure 10 [26]. The UV lamp emits UV light, which ionizes the gas molecules in the chamber. These ionized molecules generate an electrical current between the electrodes, and the magnitude of this current is directly proportional to the concentration of VOCs in the gas sample. PIDs are highly sensitive to VOCs and provide rapid responses, making them valuable in various applications. However, they come with some drawbacks, such as the high lamp replacement cost and sensitivity to environmental factors like humidity and temperature [27].
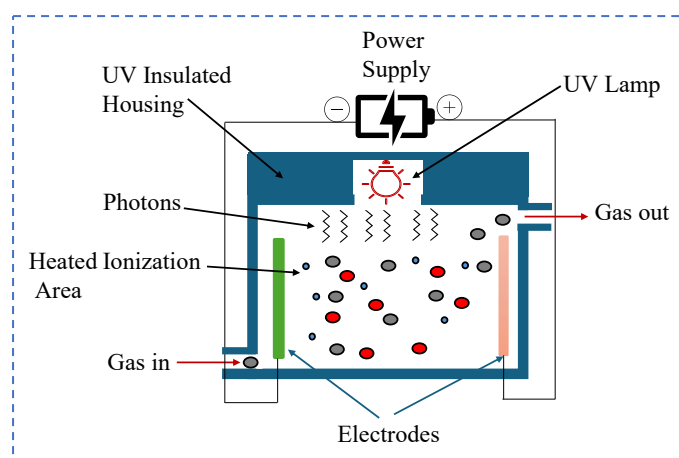
Figure 10. Schematic representation of a photoionization detector.

The study by Prestage and colleagues focused on the selective detection of VOCs using a PID paired with a nanoporous silica concentrator [28]. They aimed to detect isopropanol (IPA) and 1-octene from a mixed sample. The results indicated that the system effectively distinguished between the two VOCs based on their desorption temperatures [28]. In their experiment, VOCs were first adsorbed onto the nanoporous silica at 5 °C for five minutes. Following this, the temperature was gradually increased to 70 °C, causing the VOCs to desorb and be detected by the PID. Due to its polar nature, the IPA desorbed at a higher temperature than the non-polar 1-octene [28]. Additionally, the PID response was modeled to accurately determine the individual concentrations of each VOC, achieving detection limits of under 10 parts per billion by volume (ppb$_v$) and linearity errors of less than 1% [28]. Further, the study included a demonstration of separating a mixture of benzene and o-xylene, showcasing the system's capability to detect chemically similar compounds.

2.10. Gas Chromatography (GC)

Gas chromatography (GC) analyzers are sophisticated instruments used to separate and measure the components of a gas mixture. They consist of several key components: an injector, a chromatographic column, a carrier gas system, and a detector, all housed in a controlled environment, as illustrated in Figure 11 [29]. The process begins with the injection of a gas sample into the chromatographic column. As the sample travels through the column, its components are separated based on their interactions with the column material. The separated components are then detected and quantified by the detector. This method is highly accurate and can detect very low concentrations of gases, making it suitable for analyzing complex mixtures. However, GC analyzers are expensive, require skilled operation, and are bulkier compared with other types of gas sensors.
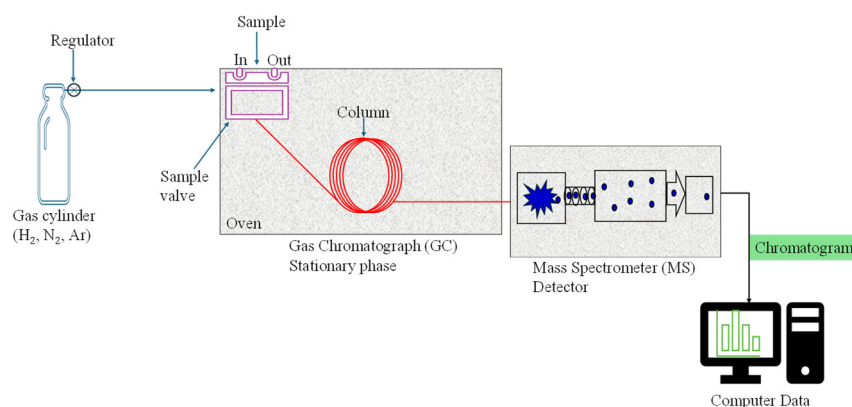
Figure 11. Schematic representation of a GC-MS analyzer.

A study by Aghili et al. investigated the detection of sesame oil adulteration using electronic nose (e-nose) technology and gas chromatography–mass spectrometry (GC-MS) [30]. The researchers introduced varying proportions of soybean and corn oils into sesame oil and conducted analyses, identifying 11 major VOCs that accounted for 82–91% of the total composition [30]. They utilized principal component analysis (PCA) and linear discriminant analysis (LDA) to visualize the adulteration levels detected by the e-nose, achieving sensitivity and specificity values of 0.987 and 0.977 with the support vector machine (SVM) method and 0.949 and 0.953 with the artificial neural network (ANN) method [30]. The findings demonstrated that e-nose technology is a rapid and effective approach for detecting sesame oil adulteration, with GC-MS providing corroborative chemical evidence.

2.11. Chemiresistor Gas Sensors

Recent advancements in nanotechnology have led to significant improvements in gas sensor technology, particularly with regard to chemiresistors that can work at room temperature. Chemiresistors offer several advantages: they are energy efficient, have a simple design, are safe to use, and can be integrated into various settings, from industrial plants to urban environments and homes. These sensors can detect even low concentrations of harmful gases in ppm and ppb, enabling quick responses to air quality issues by providing timely warnings [31,32]. The shift toward chemiresistor gas sensors is driven by their distinct advantages over other gas-sensing techniques, particularly in terms of sensitivity, simplicity, cost-effectiveness, room-temperature operation, and potential for miniaturization. The increasing number of scientific papers on polyaniline sensors, chemiresistors, and room-temperature gas sensors over the past twenty years demonstrates the increasing interest in and relevance of this research field (see Figure 12b–d).
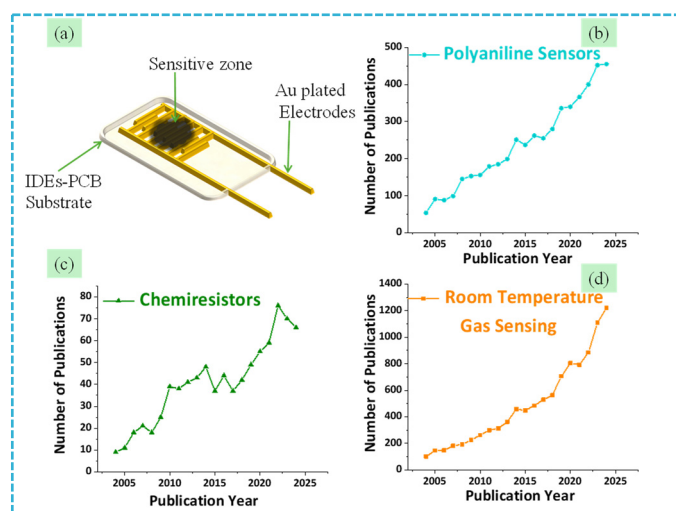
Figure 12. Schematic diagram of a chemiresistor (**a**). Publication trends in polyaniline sensors (**b**); chemiresistors (**c**); and room-temperature gas sensors (**d**) from 2004 to 2024 (based on a Scopus 15 January 2025.

Chemiresistor gas sensors operate based on the principle that the electrical resistance of a material changes in the presence of specific gases, allowing for the detection of various analytes with acceptable sensitivity and selectivity. These sensors are relatively simple in design, typically consisting of a sensing material deposited on a substrate with interdigitated electrodes, which facilitates ease of manufacturing and integration into electronic systems (Figure 12a). Moreover, chemiresistors are generally more cost-effective due to the use of inexpensive materials and straightforward fabrication processes such as printing or coating techniques. Their low power consumption is particularly beneficial for portable and battery-operated devices [31–33].

Wang and colleagues investigated a flexible and highly sensitive NH_3 sensor based on a 1D/2D heterostructured WS_2@PANI composite [34]. The synthesis method involved an in situ polymerization of aniline in the presence of WS_2 (tungsten disulfide) nanosheets. After polymerization, the composite was centrifuge washed and vacuum dried to obtain the final WS_2@PANI material [34]. Transmission electron microscopy (TEM) images revealed the fibrous structure of the composite, with PANI effectively inserted into the interlayers of the WS_2 sheets, creating a well-defined 1D/2D heterostructure. The interfacial interaction between PANI and WS_2 contributed to the composite's unique properties. In terms of gas-sensing results, the WS_2@PANI-based sensor exhibited remarkable sensitivity to NH_3, showing a high response of 216.3% to 100 ppm NH_3 [34]. The sensor's response time was 25 s, and the recovery time was 39 s. Importantly, these excellent gas-sensing characteristics were achieved at room temperature. This innovative approach holds promise for practical applications in gas sensing for environmental monitoring [34].

Despite their limitations, such as sensitivity to environmental conditions, reduced selectivity, and degradation over time, chemiresistor gas sensors remain a preferred option in a wide range of industries [35]. Their affordability and versatility make them an attractive option compared with pricier and more complex gas-sensing technologies, as outlined in Table 2. These advantages promote their use in environmental monitoring, industrial safety, and healthcare diagnostics. A chemiresistor's quality depends on the material's thickness, roughness, and composition [36]. Research indicates that gas sensors with thin and elongated shapes, including porous nanofibers, nanowires, nanoribbons, and nanotubes, are better at detecting gases with higher accuracies. These shapes offer more surface area for the gas to adhere to and react with [36,37].

Table 2. Comparison of gas sensor technologies.

Gas Sensor Type	Working Principle	Advantages	Disadvantages	Source
Catalytic Gas Sensor	Measures change in resistance due to catalytic reactions between gas molecules and a heated catalyst surface.	- High sensitivity - Fast response time - Wide range of detectable gases - Simple installation	- Requires high operating temperatures - Susceptible to poisoning - Oxygen-dependent detection - Catalyst contamination	[7,8]
Thermal Conductivity Gas Sensor	Measures changes in thermal conductivity between a reference gas and the target gas.	- Long-term stability - Low power consumption - Simple fabrication - Low cost and longer lifespan	- Limited selectivity - Insensitivity to ambient conditions - High-temperature operation - Limited detection range	[38]
Electrochemical Gas Sensor	Gas molecules cause electrochemical reactions at electrode surfaces, producing a current or voltage change.	- High sensitivity - Selectivity through membrane design - Real-time monitoring - Miniaturization potential	- Utilizes liquid electrolytes - Limited lifetime - Poor sensor stability - Expensive fabrication	[12]
Optical Gas Sensor	Measures changes in light absorption, emission, or scattering caused by gas molecules.	- High sensitivity - Wide dynamic range - Non-intrusive - Multiplexing capabilities	- Expensive instrumentation - Vulnerable to environmental conditions - Limited to line-of-sight detection - Complex data analysis	[39]
Infrared Gas Sensor	Measures changes in the absorption of infrared radiation by gas molecules.	- High sensitivity - Selectivity through wavelength specificity - Remote sensing capability - Low power consumption	- Limited to specific gases - Expensive instrumentation - Complex and bulky instrument - Interference from overlapping gas spectra	[40]
Semiconductor Gas Sensor	Gas molecules adsorb onto a semiconductor surface, changing its electrical conductivity.	- High sensitivity - Miniaturization potential - Low cost - Simple in operation - Wide dynamic range	- Cross-sensitivity - Susceptible to humidity - Calibration required - Degradation over time - High-temperature operation	[41]
Acoustic Wave Gas Sensor	Gas molecules induce mechanical waves in a piezoelectric material, leading to changes in wave properties.	- High sensitivity - Fast responsiveness - Real-time monitoring - Low power consumption	- Temperature and humidity dependence - Limited to certain gas types - Sensitivity to surface contamination	[42]

Table 2. *Cont.*

Gas Sensor Type	Working Principle	Advantages	Disadvantages	Source
Thin-Film Bulk Acoustic Resonator	Operates by converting electrical energy into mechanical energy using a piezoelectric thin film.	- Small size - Low insertion loss - Low power consumption - High frequency	- Costly fabrication processes - Sensitivity to temperature changes that can affect performance and accuracy - Limited choices of piezoelectric materials	[43]
Photoionization Detector	Uses UV light to ionize gas molecules, generating an electrical current proportional to the VOC concentration.	- High sensitivity to VOCs - Rapid response time - Non-destructive analysis - Versatile applications	- High cost of lamp replacement - Sensitivity to environmental factors like humidity and temperature - Limited detection range for certain gases - Regular maintenance required	[26,27]
Gas Chromatograph	Separates and measures gas mixture components by injecting a sample into a chromatographic column, where components are separated based on their interactions with the column material.	- High sensitivity and resolution - Ability to analyze complex mixtures - Rapid analysis time - High accuracy and precision	- Expensive equipment - Requires skilled operation - Limited to volatile and thermally stable compounds - Bulkier compared with other gas sensors	[29,30]
Chemiresistor	Gas molecules adsorb onto a chemically sensitive film, changing its resistance.	- High sensitivity - Simple design and fabrication - Low cost - Rapid response time - Wide range of detectable gases - Room-temperature operation - Miniaturization potential	- Cross-sensitivity - Limited selectivity - Degradation over time - Requires calibration	[44,45]

3. Polymer-Based Gas-Sensing Materials

In 1977, the ground-breaking discovery by the American scientists Alan MacDiarmid and Alan Heeger, and a Japanese researcher, Hideki Shirakawa, revealing that polyacetylene (PA) could exhibit metallic conductivity when chemically doped sparked a revolution in materials science [46]. This transformative breakthrough not only led to the development of conductive polymers (CPs), which was accompanied by a Nobel Prize in chemistry in 2000, but it also opened up a world of possibilities for the application of conducting polymers in various technologies [47]. The potential of scientific breakthroughs to inspire and transform our understanding of the world is truly remarkable. Over time, researchers have harnessed the unique properties of conducting polymers such as their ability to conduct electricity and to undergo reversible chemical reactions. In recent years, gas-sensing applications have sparked significant interest in both intrinsically conducting polymers (ICPs) and non-intrinsically conducting polymers (NCPs). ICPs, with their intrinsic electrical conductivity arising from conjugated π-electron systems along the polymer backbone, are particularly promising in gas sensing due to their unique electrical properties [48]. Commonly used ICPs in gas-sensing applications include PANI [49], polypyrrole (PPy) [50], polythiophene (PTh) [51], poly (3,4-ethylene dioxythiophene) (PEDOT), and polyacetylene (PA) [52] (see Figure 13).
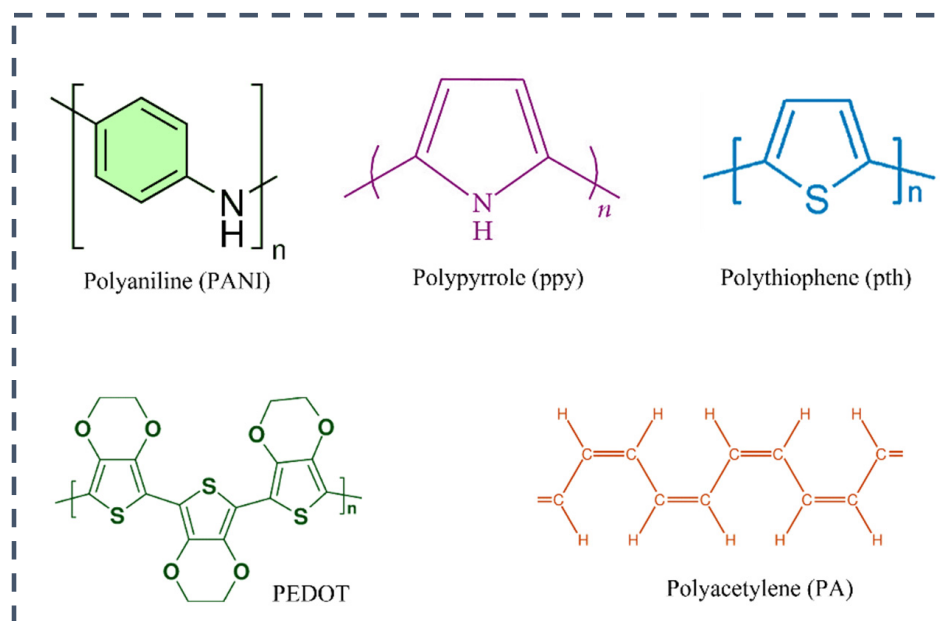
Figure 13. Schematic examples of ICPs [48].

On the other hand, NCPs, which are typically insulators or semiconductors, necessitate the incorporation of conductive fillers or specific treatments to acquire conductive properties. In the gas-sensing context, NCPs do not conduct electricity on their own; these include polystyrene (PS), polyvinyl chloride (PVC), polyethylene (PE), polypropylene (PP), polycarbonate (PC), polymethyl methacrylate (PMMA), polytetrafluoroethylene (PTFE), polyethylene terephthalate (PET), polyamide (Nylon), and polyurethane (PU). These polymers can be made conductive and are frequently utilized in composite materials by incorporating conductive fillers such as carbon nanotubes, graphene, carbon black, or metal nanoparticles embedded within the polymer matrix. Additionally, NCPs can be functionalized with specific chemical groups to interact with target gas molecules, inducing changes in the electrical properties of the polymer when exposed to gases [48,53,54].

ICPs, with their unique structures and chemical properties, hold great promise in the field of gas sensing. Their adaptability and favorable sensing characteristics, including

flexibility, easy synthesis, and high surface area, enhance their utility in gas sensing. Their structural flexibility allows them to undergo conformational changes in the presence of different gases, leading to variations in their electrical properties. This adaptability enables them to respond effectively to the environment, thereby boosting their gas-sensing characteristics at room temperature. Additionally, the high surface area of ICPs facilitates a greater interaction with gaseous molecules, leading to enhanced sensitivity in gas-sensing applications. Their flexible and porous structures allow for the efficient adsorption and desorption of gas molecules, contributing to their ability to detect and differentiate between different gases. Importantly, conductive polymers demonstrate the ability to detect VOCs at low temperatures and are less susceptible to degradation or other chemical reactions, further enhancing their potential in gas sensing. These unique properties of conductive polymers reassure us of their potential in gas-sensing applications [36,53,55].

3.1. Methods of Synthesizing Conducting Polymers

Conducting polymers (CPs) can exhibit a wide range of conductivity levels, from semiconductive to insulating, which can be achieved through a process called doping. This process involves transitioning the polymers from an insulating state to a metallic form by modulating the π-electronic system through oxidation or reduction processes (p-doping and n-doping). This can be achieved through either chemical or electrochemical means [56]. In the synthesis of conducting polymers for chemiresistive applications, a wide variety of methods are commonly used, each offering unique advantages. Electrospinning enables the production of conducting polymer nanofibers from a polymer solution by applying a high voltage to a droplet of polymer solution at the tip of a needle, which causes the droplet to deform into a cone and eject a polymer jet. The jet is stretched, dried by the electric field, and collected on a grounded substrate [43,57]. Self-assembly techniques create well-organized conducting polymer structures by controlling intermolecular interactions. Chemical oxidation involves the oxidative polymerization of monomers using chemical agents, enabling easy synthesis and tunable properties [57]. Electrochemical polymerization enables the electrodeposition of conducting polymers from monomer solutions, providing precise control over film thickness and structure [58]. Vapor phase synthesis offers advantages in terms of uniformity and scalability by involving the vaporization and polymerization of monomers on a substrate surface. Hydrothermal and solvothermal methods utilize high-temperature reactions in aqueous or organic solvents, resulting in well-defined polymer structures [59]. Template-assisted synthesis involves the use of templates to guide the polymerization process, leading to ordered nanostructures [48,59,60]. Photochemical methods utilize UV light to initiate polymerization, allowing precise spatial control and patterned deposition [61]. Solid-state synthesis involves the grinding or heating of solid precursors to synthesize conducting polymers. Lastly, plasma polymerization induces polymerization on surfaces through plasma discharges, yielding thin films [62,63]. These diverse methods offer flexibility, enabling the tailoring of conducting polymer properties for specific chemiresistive sensor applications.

3.2. Preparation of Conducting Polymer Thin Films

When depositing conducting polymers for gas-sensing applications, various methods are commonly employed. Each method offers unique advantages and provides precise control over film thickness. The thickness of the film significantly impacts the performance of a gas sensor. A thinner film typically results in faster response and recovery times due to the shorter diffusion path for gas molecules to reach the sensing material. On the other hand, a thicker film can offer higher sensitivity by providing a larger amount of sensing material for interaction with the gas molecules, although this may lead to slower response and

recovery times. Therefore, the choice of film thickness is crucial and depends on the specific requirements of a gas-sensing system. For example, electrochemical deposition allows the adjustment of the total charge passed through an electrochemical cell during the film growth process [64]. Dip-coating involves immersing a substrate in a solution containing the conducting polymer, resulting in a thin film deposition [65]. Spin-coating utilizes a rotating substrate to spread the polymer solution evenly, creating a uniform film [66]. The Langmuir–Blodgett technique entails transferring a monolayer of conducting polymer from a water surface onto a solid substrate [67,68]. Similarly, Layer-by-Layer Self-Assembly enables the deposition of alternating layers of conducting polymer and oppositely charged species, yielding precise control over film thickness [69]. Vapor deposition polymerization involves the vapor-phase polymerization of monomers on the substrate surface, leading to the formation of a thin film [70]. Drop-coating involves dropping a solution containing the polymer onto the substrate, which subsequently leads to film formation [71]. Lastly, electric field-induced electrochemical polymerization utilizes an electric field to guide the polymerization process, resulting in a deposited film [72].

3.3. Application of CPs in Gas Sensing

In gas-sensing applications, CPs are essential for detecting various substances in the air. The highly porous nature and nanostructure of CPs such as nanorods, nanoribbons, nanotubes, and nanofibers influence their sensitivity to gas, enabling effective absorption of gas molecules and providing a large surface area for enhanced gas molecule absorption [35,73]. When in contact with gas or VOCs, CPs undergo changes in their physical properties, which can be modified through polymer doping to influence the sensor's capacity to detect different gases. The introduction of chemical compounds or structures within the conducting polymers facilitates the transfer of electrical charges and significantly impacts the physicochemical properties of the conducting polymers, allowing for independent gas detection possible at room temperature. These compounds can be formed through the acceptor or donor doping process and significantly influence the behavior of the conducting polymers in response to different gases, making them essential for efficient gas sensors. The reversible doping and de-doping mechanism of conducting polymers in response to specific gases can be used to detect gases such as water vapor, hydrocarbons, acetone, and organic acids [49,56,74]. Additionally, conducting polymers display swelling or adsorption behaviors upon contact with gases, separating the conductive networks of the sensing material and thus enabling the detection of specific gases. This capability makes conducting polymers essential for efficient gas sensors, as they can effectively detect a variety of important gases. However, to fully harness this potential, understanding the swelling behavior associated with organic vapors and its impact on the sensing properties is crucial for the development of effective gas sensors that rely on conducting polymers [48,74,75].

4. The Role of PANI in Gas Sensing: An Overview

PANI is one of the oldest and most researched intrinsically conducting polymers (ICPs). It is similar to polypyrrole (PPy) but has more advantages such as low-cost monomer, better environmental stability, easier synthesis, and higher electrical conductivity. PANI can take on various forms depending on its degree of oxidation [65]. These forms are distinguished by distinct colors that correspond to their oxidation states. For example, PANI is transparent when fully reduced (leucoemeraldine base, -NH-), violet when fully oxidized (pernigraniline base, -N=), and blue when half-oxidized (emeraldine base, -NH- and -N=) (Figure 14). The color variation of PANI can be advantageous in gas sensing due to its reversible oxidation state. Unlike the other forms, the emeraldine base form is particularly valuable, as it can acquire conductivity when doped with acids to form the

emeraldine salt form. The conductivity of PANI is contingent upon the equilibrium between the oxidized-quinonoid and reduced-benzenoid units in the polymer. This reversible oxidation state makes PANI useful in gas-sensing applications, as it can effectively interact with gas molecules and undergo changes in its electrical conductivity, providing a basis for gas detection and sensing [76].
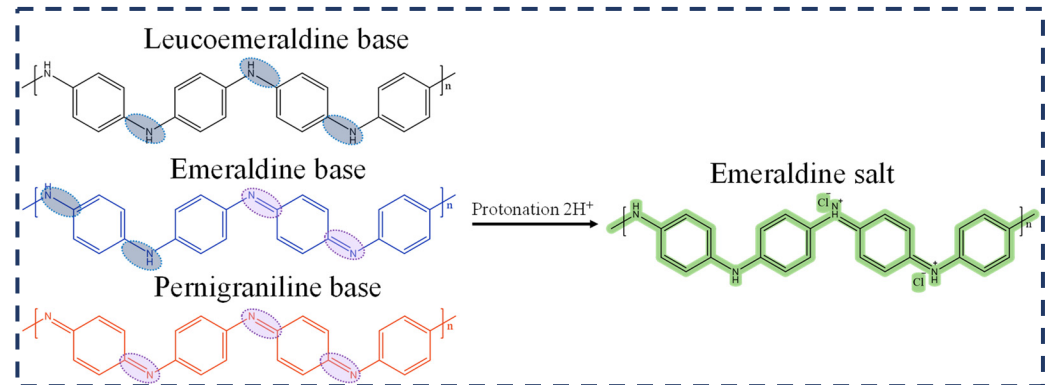
Figure 14. Various primary forms of PANI and the formation of conductive PANI.

4.1. PANI-Based Nanocomposite Sensors

A nanocomposite is a material comprising two or more components with distinct properties, at least one of which has nanoscale dimensions. Nanocomposites can demonstrate novel or enhanced properties different from those of the individual components, as depicted in Figure 15. The objective is to create a material that combines the strengths of each element and provides new opportunities for various applications. However, PANI faces challenges in gas sensing due to limitations such as mechanical instability, resulting in slow gas response times, extended recovery times, and a lack of specificity. To address these shortcomings, PANI can be combined with other materials to form polymeric nanocomposites, thereby improving its sensing capabilities and efficiency [77]. Materials such as carbon nanostructures, metal nanoparticles, metal oxides, metal chalcogenides, and other polymers can be incorporated into PANI to produce nanocomposites with diverse and enhanced features for gas-sensing applications, which will be discussed in the following sections.
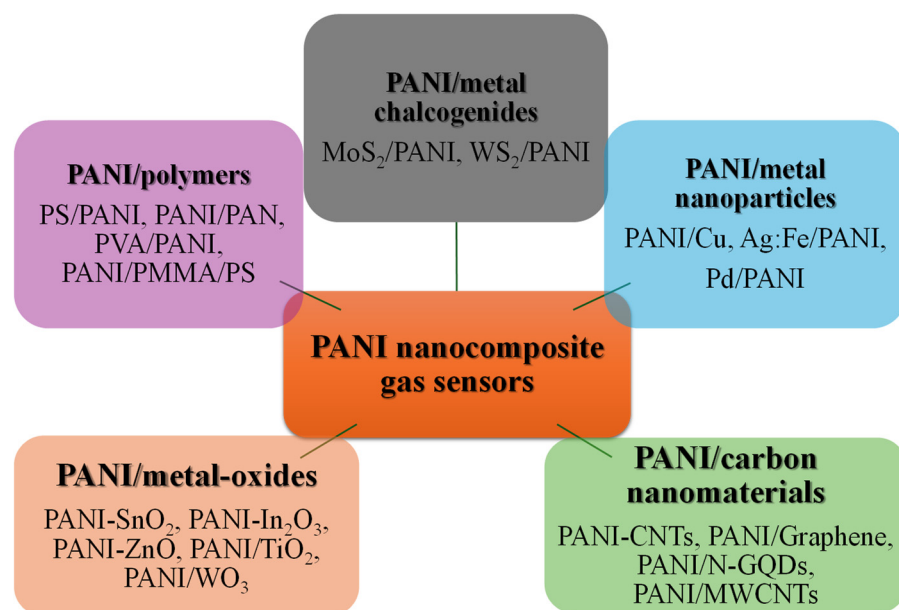
Figure 15. Gas-sensing materials based on PANI nanocomposites.

4.2. Gas Sensing with PANI/Polymer Blend Nanomaterials

Li and colleagues compared PANI nanocomposites doped with different protonic acids: serine, nitric acid (HNO_3), and tartaric acid [78]. The study showed that the dopant plays a critical role in determining the morphology and gas-sensing performance. The PANI nanocomposites were synthesized using chemical oxidative polymerization. Analysis revealed that the composites had significantly different nanostructures. PANI@HNO_3 exhibited a granular morphology, while PANI@Tartaric acid had smaller particles at the nanoscale level, and PANI@Serine showed a unique petal-shaped nanostructure performance. The PANI nanocomposites were tested for their ability to sense NH_3 gas at room temperature (25 ± 2 °C) with concentrations ranging from 10 ppm to 1000 ppm. Among the sensors tested, the PANI@Serine sensor showed the highest sensitivity to NH_3, with a response of 6.12 at 16 ppm of NH_3, and it had a low detection limit of 10 ppm. This sensitivity was 4.29 times greater than that of the PANI@Tartaric acid sensor and 5.81 times higher than the PANI@HNO_3 sensor. Additionally, the PANI@Serine sensor demonstrated significantly shorter response and recovery times of 170 s and 304 s, respectively, which were 87 s and 63 s faster than those of the PANI@HNO_3 sensor, respectively. The effect of relative humidity (RH) was examined from 25% to 72%, and the response value of the PANI@HNO_3 sensor continued to increase. This behavior suggested a synergistic interaction between NH_3 and H_2O molecules on the sensor surface, leading to the reactions shown in Equations (1) and (2) [78]:

$$NH_3 + H_2O \leftrightarrow NH_4{}^+ + OH^- \tag{1}$$

$$NH_3 + PANIH^+ \leftrightarrow NH_4{}^+ + PANI \tag{2}$$

These reactions caused NH_3 molecules to consume holes in the polymer sensor. Additionally, unstable H_2O molecules became adsorbed onto the surface, causing the polymer to expand and become more disordered, thereby inhibiting carrier movement and increasing sensor resistance. The dual role of H_2O molecules in the adsorption of NH_3 also explained the observed changes in the response resistance of the PANI@Tartaric acid sensor [78]. The baseline drifts observed during testing were attributed to incomplete desorption of NH_3 molecules from the sensor surface. The researchers used density functional theory (DFT) calculations to explore NH_3 adsorption on various PANI nanocomposites. They found that PANI@Serine exhibited superior adsorption compared with PANI@HNO_3 and PANI@Tartaric acid due to the enhanced interaction with NH_3 molecules facilitated by serine's functional groups, leading to improved sensitivity. Additionally, the team highlighted the environmentally friendly approach of using amino acids as doping agents to enhance gas sensor performance, emphasizing its significance for sustainable sensor technologies [78].

Lv and colleagues developed a flexible NH_3 gas sensor using a poly (styrene sulfonic acid) (PSS)-doped PANI composite with a polyvinylidene fluoride (PVDF) membrane as the substrate [79]. The sensor was fabricated through an in situ polymerization process, starting with the protonation of aniline in a hydrochloric acid solution. The PVDF membrane was immersed in this solution, allowing aniline molecules to react on its surface. Following this, ammonium persulfate (APS) was introduced as the oxidizing agent, initiating the polymerization of aniline and forming PANI nanoparticles on the porous structure of the PVDF membrane. Subsequently, these PANI-coated membranes were treated with a poly (styrene sulfonic acid) (PSS) solution, resulting in the formation of the PSS-PANI/PVDF composite. The final product was then prepared for sensing applications by applying a silver interdigital electrode (Ag-IDE) using a screen-printing method. The PVDF membrane used as the substrate had a porous structure with pore sizes ranging between 1 and 15 μm,

providing excellent air permeability for gas-sensing applications. The PANI nanoparticles uniformly coated both the surface and inner micropores of the PVDF membrane, effectively increasing the film's surface area. The addition of PSS to the PANI/PVDF composite further modified the morphology, creating a 3D hierarchical porous structure that increased the contact area with gas molecules and enhanced the sensitivity to NH_3 molecules. The researchers evaluated the gas-sensing performance of the PSS-PANI/PVDF composite by exposing it to NH_3 concentrations ranging from 0.1 to 10 ppm at room temperature. The sensor exhibited remarkable sensitivity, achieving a maximum response of 649% to 10 ppm NH_3 and a significant response of 9.4% to 0.1 ppm NH_3 (Figure 16a). The response and recovery times for the sensor were recorded as 160 s and 400 s, respectively, for an NH_3 concentration of 1 ppm [79]. Furthermore, the sensor showed excellent reproducibility, maintaining consistent response and recovery characteristics over multiple testing cycles, as shown in Figure 16b. The inclusion of PSS in the composite was found to enhance the sensitivity of the sensor significantly. Specifically, a 1 wt% concentration of PSS resulted in a 2.8-fold improvement in sensor response compared with the undoped PANI/PVDF composite. The sensor also exhibited excellent stability under various environmental conditions, maintaining its performance with less than 5% response degradation after 30 days of testing. The NH_3 sensing mechanism of the PSS-PANI/PVDF sensor was primarily due to the interaction between NH_3 gas molecules and the PANI matrix. This interaction resulted in a doping–dedoping process, causing the polymer's electrical conductivity to change. The PSS dopant, with its high proton conductivity, provided additional active sites for gas adsorption, enhancing the sensor's sensitivity to NH_3. The hierarchical porous structure facilitated efficient gas diffusion and interaction with PANI nanoparticles, leading to faster response and recovery times. These findings suggested that PSS-PANI/PVDF composite sensors could be effectively employed in wearable devices for real-time monitoring of NH_3 in various environments, including industrial applications and health monitoring such as detecting NH_3 in human breath [79].
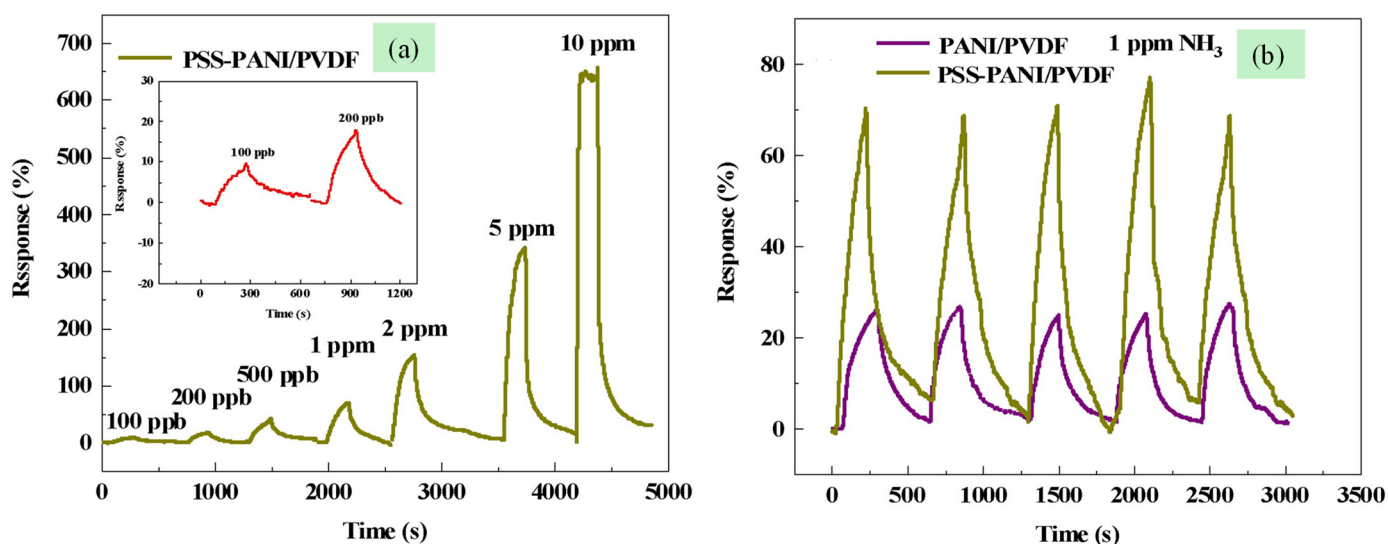
Figure 16. Dynamic response of PSS-PANI/PVDF to 100 ppb–1000 ppm NH_3 at room temperature under 25% RH (**a**); repeatability tests for PANI/PVDF and PSS-PANI/PVDF to 1 ppm NH_3 (**b**). Reprinted with permission from [79], copyright 2024 Elsevier.

Devi and colleagues synthesized PANI/PVA conductive hydrogels using repetitive freezing–thawing and in situ polymerization methods to detect NH_3 at room temperature [80]. The number of freezing–thawing cycles determined the microstructure of the resulting hydrogels, influencing pore size and network interlacing. Using a freeze–thaw

process, six hydrogel samples (PPH1 to PPH6) were prepared, each undergoing a different number of cycles. The morphological characteristics revealed a significant impact of the repetitive cycles on the pore size and interlacing network structure. As the number of cycles increased, there was a significant expansion in the pore size, and the interlacing network developed a scale-like leaf structure [80]. Among the different hydrogel samples, PPH4 showed the highest sensitivity to NH_3, attributed to its larger specific surface area, which enhanced gas absorption and diffusion. The sensing mechanism was based on the interaction between NH_3 molecules and the doped PANI, leading to a protonation–deprotonation process (Figure 17a) [81]. When PANI comes into contact with NH_3, NH_3 molecules take on protons (H^+) from the PANI backbone, resulting in the formation of NH_4^+ ions. The process was energetically favorable and caused electrons to transfer to PANI, leading to its deprotonation [80]. As a result, the emeraldine salt form of PANI (which is conductive) was transformed into the emeraldine base form (which is non-conductive). When the concentration of NH_3 decreased, NH_4^+ ions broke down into NH_3, causing the non-conductive PANI to return to its conductive $PANIH^+$ form [69]. This reversible process of doping and dedoping, or protonation and deprotonation, supports the operation of most PANI-based sensors. The electron dynamics involved in this mechanism allow PANI sensors to exhibit a sensitive response to NH_3. Equation (2) is a summary of the anticipated interaction between PANI and NH_3 [80].
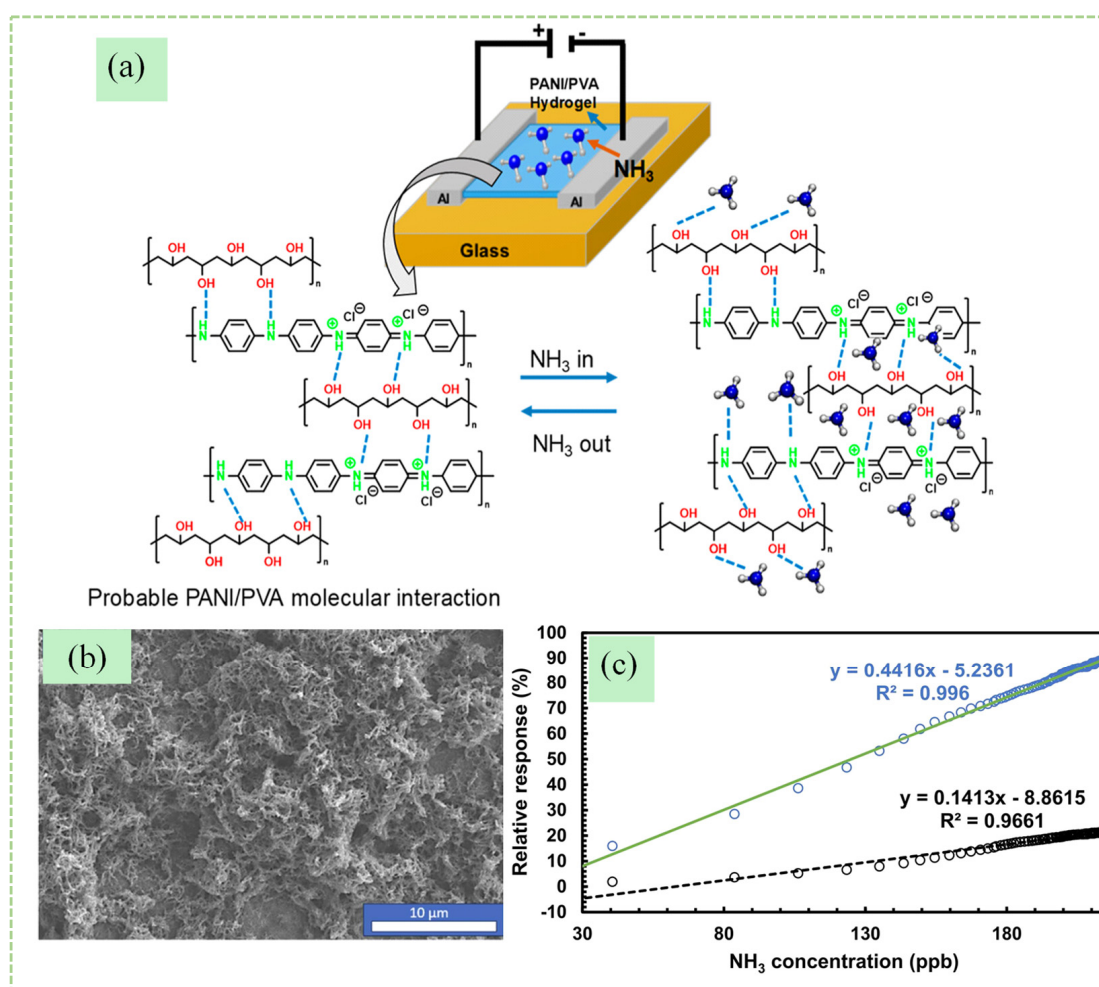
Figure 17. Proposed sensing mechanism of PANI/PVA sensor (**a**). Reprinted with permission from [80], copyright 2024 American Chemical Society. SEM image of Ani:AF 50:50 (**b**); calibration curve of the Ani:AF 50:50 sensor obtained from one cycle of measurements (T = 22.5 °C. RH = 48%) (**c**). Reprinted with permission from [81], copyright 2024 Elsevier.

PANI and PANIH$^+$ represent PANI's undoped and doped forms, respectively. The PPH4 sensor demonstrated a detection limit of 1 ppm, with response and recovery times of 25–45 s and 10 s, respectively. Its sensitivity increased with higher NH$_3$ concentrations due to hydrogen bond formation, and it showed no significant sensitivity change when exposed to CO$_2$ and NO$_2$ with NH$_3$. The hydrogel sensor's response to RH% was tested at 50 °C, and the response showed a continuous decrease in resistance as RH% increased from 15% to 90%. The sensor also exhibited excellent stability over three months without significant degradation [80].

Kayishaer et al. studied the synthesis of fluorinated PANI films through the electrochemical oxidation of 2-fluoroaniline in different acidic environments, including sulfuric acid (H$_2$SO$_4$), camphorsulfonic acid (CSA), and perchloric acid (HClO$_4$) [81]. Their findings indicated that the properties of the synthesized polymer films were markedly influenced by the type of acid used during the electrochemical process, with perchloric acid producing films with greater thickness and conductivity, effectively enhancing gas-sensing performance. The scanning electron microscope (SEM) images of PANI films showed a spongy, fibrous architecture, while the fluorinated PANI films had a denser morphology with micrometric globule clusters (Figure 17b). Fluorine integration significantly influenced the film morphology. Films with a higher aniline-to-fluoroaniline (Ani:AF) ratio of 75:25 resembled pure PANI structures but with fewer and smaller pores. Films with ratios of 50:50 and 25:75 had more compact structures without the pores and fibers seen in PANI. The researchers found that the fluorinated PANI sensors were highly sensitive to NH$_3$ at concentrations from 40 to 1000 ppb at 48% RH and 22.5 °C. They consistently returned to their baseline resistance after each exposure, even with NH$_3$ concentrations as high as 1000 ppb, indicating efficient desorption of gas molecules [81]. The poly(aniline/2-fluoroaniline) sensor demonstrated a sensitivity of 0.44% per ppb (Figure 17c), while the PANI-based sensor exhibited a sensitivity of 139 ± 28% per ppm. The repeatability of the sensor responses was evaluated over five successive cycles of NH$_3$ exposure at a concentration of 200 ppb. The poly(aniline/2-fluoroaniline) films demonstrated an average response variation of 10 ± 3%, while the PANI films showed a variation of 7 ± 2%. Regardless of the humidity level, the poly(aniline/2-fluoroaniline)-based sensors consistently responded more than the PANI-based sensors. The sensitivity of both sensor types was only marginally affected by variations in humidity when the RH exceeded 20%, regardless of whether the humidity increased or decreased. The limit of detection (LOD) was determined to be as low as 4 ppb, and the sensors showed a linear response over a wide range of NH$_3$ concentrations, from 10 ppb to 50 ppm, with the resistance increasing rapidly at higher NH$_3$ concentrations, ensuring precise and reliable detection [81].

In a study by Chaudhary, nanospheres of polypyrrole (PPY), polyaniline (PAN), and polyaniline-co-pyrrole (PAP) were synthesized using a template-free electrochemical oxidative method [82]. The researcher deposited the polymeric films on an ITO-coated glass substrate in sulfuric acid using a three-electrode cell and fabricated chemiresistor devices in m-cresol. The synthesized PPY, PAN, and PAP nanospheres had diameters of approximately 500 nm, 100 nm, and 50 nm, respectively. The PAP nanospheres had the highest specific surface area (282 m^2/g) compared with PPY (82 m^2/g) and PAN (204 m^2/g). The PAP chemiresistor had the lowest conductivity at room temperature (9.5×10^{-5} S/cm) compared with PAN (1.4×10^{-4} S/cm) and PPY (2.2×10^{-4} S/cm) due to the presence of heterodia d units disrupting long-range conjugation. Both PAP and PAN chemiresistors increased conductivity with temperature, indicating semiconducting behavior. Mott's variable range hopping (VRH) model determined that polarons and bipolarons governed the charge transport mechanism in these nanospheres. The PAP chemiresistor exhibited the highest sensing response (6.1%) to 5 ppm of SO$_2$ at room temperature, with a delayed

saturation time compared with the PAN (2.9%) and PPY (1.1%) chemiresistors. The lower conductivity in the PAP chemiresistor increased the likelihood of polymer chain oxidation by SO_2. Additionally, the PAP chemiresistor maintained a stable response over three weeks in environmental conditions with minimal decline in sensing performance. The response to SO_2 was reversible over multiple exposure cycles. It also demonstrated the highest response signal to SO_2 when exposed to 5 ppm concentrations of selected reducing and oxidizing gas analytes at room temperature, highlighting its selectivity [82].

4.3. Gas Sensing with PANI/Carbon Nanomaterials

Li et al. developed an NH_3 gas sensor by creating a nanocomposite of PANI and graphitic carbon nitride (g-C_3N_4) [83]. The process involved exfoliating g-C_3N_4 hydrothermally and then polymerizing PANI in situ. Based on the doping molar concentration, the prepared PANI/g-C_3N_4 nanocomposites were designated as PCN (5), PCN (10), PCN (20), PCN (30), and PCN (40). Sensor devices were fabricated by depositing the PANI/g-C_3N_4 nanocomposites on a PET fork finger electrode through electrostatic self-assembly. TEM images revealed that amorphous PANI grew on and adhered to the surface of sheet-like g-C_3N_4. Among the nanocomposites, the 30% PANI/g-C_3N_4 hybrid exhibited the highest effectiveness, with a specific surface area of 32.18 m^2/g. The sensor demonstrated heightened sensitivity to NH_3, exhibiting a response of 19.53 to 200 ppm of NH_3 at 25 ± 5 °C, which was 1.5 times greater than the response of the pure PANI sensor (12.99). Furthermore, the sensor was capable of detecting concentrations as low as 500 ppb of NH_3, with both sensors providing linear responses within the range of 0.5 to 100 ppm. The PCN 30 sensor displayed a more rapid response rate of 0.1169/ppm compared with the pure PANI sensor's rate of 0.0771/ppm, indicating its enhanced gas-sensing properties. The PCN 30 thin-film sensor exhibited faster response and recovery times for 10 ppm NH_3 at 134 s and 624 s, respectively, when compared with the pure PANI thin-film sensor, which showed times of 175 s and 631 s [83]. The improved measurements were attributed to enhanced charge transport facilitated by the structure between g-C_3N_4 and PANI. Stability tests over 21 days revealed that the response of the PCN 30 sensor to 10 ppm NH_3 initially declined slightly before stabilizing, which may be due to the deactivation of some active sites [84]. Additionally, the PCN 30 hybrid sensor exhibited strong selectivity for NH_3, attributed to the distinctive response mechanism of PANI aligning well with NH_3 as an alkaline gas. The PCN 30% hybrid sensor's ability to detect NH_3 was influenced by humidity levels (25–90% at 24 °C). As humidity increased, the sensor's initial resistance decreased, slightly improving its ability to detect NH_3 due to increased electrical conductivity. When exposed to NH_3, the sensor's resistance rapidly increased. NH_3 interaction with water molecules further improved the sensor's ability to detect NH_3 [83].

The research by Masemola et al. focused on synthesizing N-doped graphene quantum dot-modified PANI for sensing alcohol vapors at room temperature [84]. The NGQDs exhibited a dot-like structure with an average diameter of 5 nm. The fiber diameters were measured at 41 ± 10 nm for PANI and 47 ± 14 nm for the composite, indicating a denser structure attributed to strong π-interactions [84]. The BET surface area was determined to be 31.2 m^2/g for PANI and 41.0 m^2/g for the NGQDs/PANI composite. The study investigated how PANI and NGQDs/PANI composite sensors reacted to different concentrations of ethanol gas at room temperature (26 °C) and 45% RH. Both sensors showed linear responses to increasing ethanol concentrations. The NGQDs/PANI composite sensor had a 39% higher response than PANI at high ethanol concentrations due to the improved charge transfer pathways and increased surface area provided by the NGQDs (see Figure 18a). The sensor's real-time response increased linearly until saturation, followed by a decrease, indicating a reduction in available surface adsorption sites. The sensor also exhibited

response and recovery times of 85 s and 62 s, respectively (Figure 18b), while the pure PANI sensor showed times of 118 s and 80 s [84]. Additionally, the NGQDs/PANI sensor showed linear responses to methanol, ethanol, and isopropanol within the 50–150 ppm range, with specific response and recovery times for each gas. Among the gases tested, isopropanol showed the highest response signal. The difference in sensitivity was likely due to the shapes and energies of the analyte VOCs [84].
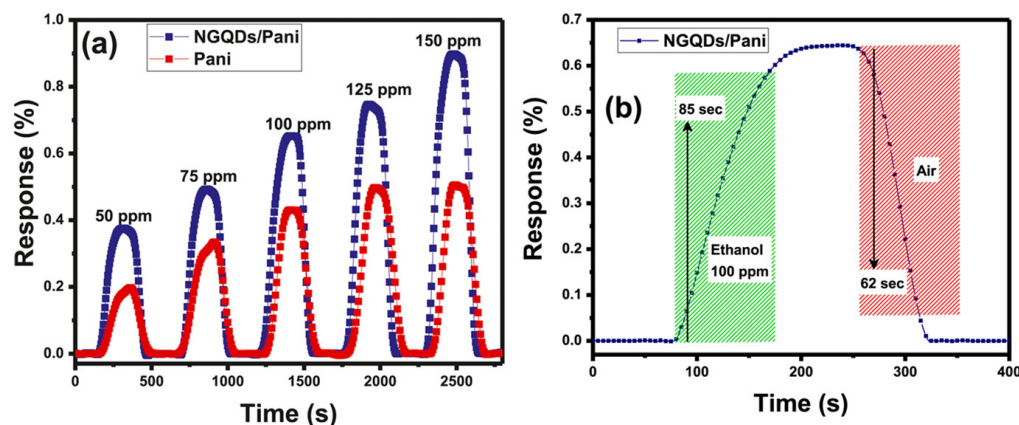
Figure 18. (**a**) Gas response of the sensors to 50–150 ppm of ethanol and response/recovery times of the NGQDs/Pani sensor at 26 °C and 45% RH (**b**). Reprinted with permission from [84], copyright 2024 Elsevier.

Chen and co-workers developed a new material for detecting NH_3 gas by applying a PANI layer to a 3D porous carbon framework to create PANI@3D C-FW composites (CPs) [85]. The 3D C-FW was produced using a freezing and drying process and was subsequently coated in situ with PANI. The PANI@3D C-FW composite polymers have a 3D porous structure with rough surfaces, distinct from the smooth surface of the pristine C-FW. The authors also investigated the selectivity response of the PANI@3D C-FW CPs sensor toward 10 ppm NH_3 and various interfering gases, including H_2, H_2S, CO, NO, NO_2, ethanol, and acetone. The results showed a significantly heightened reaction to NH_3 compared with other gases, demonstrating exceptional selectivity [86]. Further assessments involved combining 10 ppm NH_3 with the interfering gases. The sensor's reaction remained consistent when combined with pure NH_3, confirming its outstanding selectivity in the presence of interfering gases. The PANI@3D C-FW CPs proved to be stable, repeatable, and durable over repeated cycling under 10 ppm NH_3 with almost complete response and recovery [85]. The sensors also maintained a consistent response over 249 days, with similar response and recovery patterns observed on the 1st, 96th, 136th, and 249th days [85]. Changes in baseline resistance and prolonged response and recovery times were associated with adsorbed oxygen and residual NH_3 molecules [85]. The sensor's response to NH_3 decreased slightly with increasing humidity, likely because water molecules took up some NH_3 adsorption sites, but a 1% change in humidity had less impact than a 0.1 ppm change in NH_3 concentration. The sensors showed the strongest reaction to 10 ppm of NH_3 at room temperature. Additionally, a 1 °C change in temperature produced a comparable effect on the sensor's response as a 0.1 ppm change in NH_3 concentration (1.63%). The improved sensing response of PANI@3D C-FW CPs to NH_3 was due to the large specific surface area of the porous 3D C-FW, which supported PANI and provided many adsorption sites, improving NH_3 sensing [85]. Also, the π–π interactions between the 3D C-FW and PANI promoted electron sharing, enhancing charge transfer, and the presence of PANI facilitated the conversion of NH_3 molecules into NH_4^+, further improving sensor performance. The PANI@3D C-FW CPs selectively responded to NH_3 and H_2S, with resistance changes in

opposite directions when exposed to the target NH_3 and interfering H_2S. It was suggested that the H^+ ions from H_2S may have formed bonds with the amine nitrogen sites of PANI, forming new N-H bonds. This property allowed the sensor to distinguish between different gases based on their interaction with the sensing material [85].

Singh et al. designed porous PANI/phosphorus-nitrogen co-doped graphene nanocomposites for efficient room-temperature NH_3 sensing [86]. They used graphene oxide (GO) and reduced it to reduced graphene oxide (rGO) using hydrazine hydrate. They also created phosphorus–nitrogen dual co-doped graphene (PNGN) via hydrothermal treatment with diammonium hydrogen phosphate. Additionally, they synthesized PANI by polymerizing aniline monomers in a solution containing sodium chloride and hydrochloric acid. They then made the composite materials, PANI/rGO and PANI/PNGN, by blending varying concentrations of PNGN with the aniline monomer and hydrochloric acid and then carrying out polymerization. The samples PANI/PNGN 5%, PANI/PNGN 10%, and PANI/PNGN 15% were designated based on the concentration of PNGN used in the synthesis. FESEM (field emission scanning electron microscopy) images of PANI/PNGN 15% showed uniform PANI growth on the PNGN surface while maintaining the porous structure. PNGN acted as an efficient seed layer, providing active sites for PANI growth. PANI chains exhibited aromatic properties, resulting in robust interconnections with PNGN. The hybrid nanocomposite materials exhibited increased surface areas. Dynamic response curves of PANI/PNGN sensors with 5%, 10%, and 15% PNGN content were measured at NH_3 concentrations of 60, 80, and 100 ppm. The NH_3 sensing response increased with higher concentrations of PNGN. The increased sensing response observed with higher PNGN doping can be attributed to the reduced bandgap and improved conductivity, resulting in the highest response for PANI/PNGN 15%. Dynamic sensing response curves of the sensors exposed to 100 ppm NH_3 indicated response and recovery times of 21 s and 56 s, respectively, for the PANI/PNGN 15% film sensor. The sensor also showed good repeatability in response to 5 on/off cycles at concentrations of 60 and 100 ppm NH_3 gas. The results showed no significant decrease in sensing response across cycles, with the sensor consistently achieving the same maximum response upon NH_3 exposure and returning to the same minimum after NH_3 removal, thus confirming the cyclical repeatability of the device. The PANI/PNGN 15% sensor showed 70.37% selectivity for NH_3, 10.4% for methanol, 9.2% for ethanol, 5.07% for acetone, and 4.6% for chloroform at 60 ppm. The PANI/PNGN 15% sensor showed good linearity ($R^2 = 0.98642$) for NH_3 concentrations of 5 to 40 ppm. Above 40 ppm, the sensitivity increased, described by the equation $Y = 10.990767X + C$, compared with $Y = 5.60643X + C$ for the 5 to 40 ppm range. The increase was assumed to be due to higher NH_3 molecule surface coverage on PANI/PNGN 15%. The PANI/PNGN 15% nanocomposite film's sensitivity to relative humidity rapidly increased up to 60% RH, reaching a saturated value of 63.6%. The humidity test showed minimal impact on the sensor's response. A stability analysis of the fabricated devices over a six-month period revealed less than a 5% decrease in sensing response at 100 ppm of NH_3, indicating high durability [86].

When a CNT/PANI sensor is exposed to CO gas, it interacts with the gas molecules through two mechanisms: physisorption and chemisorption (Figure 19) [87]. These interactions change the sensor's conductivity. Physisorption occurs when CO gas molecules attach to the sensor's surface via weak van der Waals forces. This causes electrons to move from the CNT/PANI sensor to the CO gas molecules, leading to the spread of polarons (charge carriers) within the sensor. As a result, the sensor's resistance decreases, which means its conductivity increases. When the sensor is exposed to air, the CO gas molecules detach, and the sensor returns to its original conductivity as the polarons localize back in the PANI matrix. This process is easily reversible and does not require external energy.

Chemisorption involves the formation of stronger chemical bonds between the CO gas molecules and the sensor. Due to the co-planarity of the phenyl rings in PANI, electrons are transferred from the CNT/PANI sensor to the CO gas molecules. This increases the number of mobile charge carriers (holes) in the PANI, enhancing the sensor's conductivity [88].
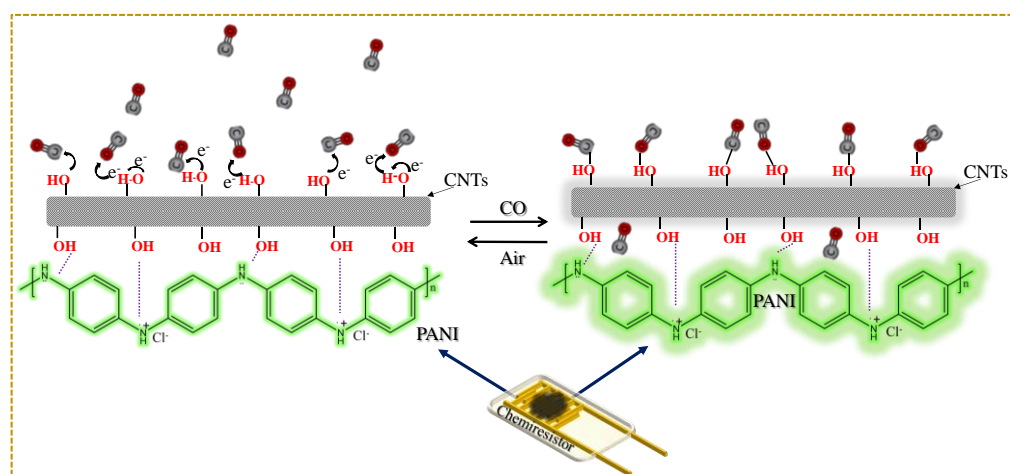
Figure 19. Sensing mechanism of CNT/PANI composite to CO gas. The image is not drawn to scale.

4.4. Gas Sensing with PANI/Metal Nanoparticles

Metal nanoparticles (MNPs), such as Cu, Ni, Pd, and Ag, can be incorporated onto PANI to enhance its gas-sensing properties. Certain metals have demonstrated the ability to improve gas sensor selectivity due to their superior gas absorption characteristics toward specific analyte gases. In a study by Adhav et al., PANI/Ag nanocomposites were utilized for rapid NH_3 detection at room temperature [89]. The nanocomposites, which consisted of PANI and Ag nanoparticles, were synthesized using in situ sonochemical oxidative polymerization methods with ammonium persulfate. The prepared PANI/Ag nanocomposites displayed enhanced gas-sensing properties due to their agglomerated fibrous structures with uniformly distributed silver nanoparticles. The concentration of silver nanoparticles significantly influenced the morphology, improving sensitivity and reproducibility. The sensor displayed a significant change in resistance with increasing NH_3 concentration, even at low concentrations. The PANI/Ag sensor produced a maximum sensitivity of 57% at 100 ppm NH_3, with a notable response of 18% at 1 ppm. The sensor's response and recovery times were influenced by NH_3 concentrations, showing a decrease in response time from 100 s at lower concentrations to 30 s at 100 ppm and an increase in recovery time from 40 to 120 s with higher NH_3 concentrations. At 100 ppm, the sensor also showed a high selectivity for NH_3 over other gases. Overall, it demonstrated exceptional long-term stability when exposed to 100 ppm NH_3 for 180 days, with less than a 5% change in its original response [89].

In research conducted by Verma, the application of PANI@Ag/Cu hybrid nanocomposites for NH_3 sensing was investigated [90]. The PANI@Ag/Cu hybrid nanocomposites were synthesized with varying concentrations of silver nitrate and copper acetate (0.15, 0.3, 0.6, 0.9, and 1.2 M), and these were designated as PANI@Ag/Cu$_1$, PANI@Ag/Cu$_2$, PANI@Ag/Cu$_3$, PANI@Ag/Cu$_4$, and PANI@Ag/Cu$_5$, respectively. The band gap values of the PANI@Ag/Cu hybrids increased with higher concentrations of silver and copper nanoparticles. The band gap of PANI@Ag/Cu$_1$ was 2.4 eV, that of PANI@Ag/Cu$_2$ was 2.6 eV, PANI@Ag/Cu$_3$ was 2.9 eV, PANI@Ag/Cu$_4$ was 3.5 eV, and PANI@Ag/Cu$_5$ had the highest band gap of 4.1 eV compared with the pure PANI band gap of 2.21 eV. Analysis of the morphology of pure PANI found it to have nanofibers approximately 100 nm in diameter and extending to several micrometers in length. In contrast, PANI@Ag/Cu$_1$ dis-

played non-agglomerated silver and copper nanoparticles that were uniformly distributed, resembling nanospheres with an average diameter of about 344 nm. The PANI@Ag/Cu$_5$ composite showed aggregated silver and copper nanoparticles incorporated within the PANI matrix, resulting in increased particle size and density. These findings highlight the influence of nanoparticle concentration on the PANI matrix's morphology and distribution. The PANI@Ag/Cu hybrid nanocomposite effectively detected NH$_3$ gas at room temperature. The PANI@Ag/Cu$_5$ composite demonstrated the highest response to NH$_3$ gas, with a value of 73% at 100 ppm, compared with 38% for pure PANI. Additionally, the sensors displayed excellent selectivity for NH$_3$ gas over other gases such as ethanol, CO, H$_2$S, and CO$_2$. The PANI@Ag/Cu hybrid nanocomposite sensors displayed faster response and recovery times compared with pure PANI. For example, the PANI@Ag/Cu$_3$ sensor had a rapid 8 s response time for 300 ppm of NH$_3$ gas and a 10 s recovery time after gas removal. Compared with pure PANI, the PANI@Ag/Cu sensors exhibited a more significant drop in resistance, indicating enhanced sensitivity to 100–300 ppm NH$_3$ [90].

When a Cu-PANI sensor is exposed to NH$_3$ gas, the gas molecules first attach to the sensor's surface through weak van der Waals forces, and then, they form stronger chemical bonds with Cu nanoparticles and the PANI matrix [91]. NH$_3$, being a reducing gas, donates electrons to the Cu-PANI sensor, primarily at the sites where copper nanoparticles are present. This electron transfer reduces the number of charge carriers (polarons) in the PANI matrix, leading to an increase in the sensor's resistance and a decrease in its conductivity [92]. This change in conductivity serves as a measurable signal indicating the presence of NH$_3$ gas. Additionally, NH$_3$ can be converted to ammonium ions (NH$_3$ + H$^+$→NH$_4^+$), which further interact with the sensor. When the sensor is exposed to air, the NH$_3$ molecules detach, and the sensor regains its original conductivity, as the electrons are removed and the holes in the PANI matrix are restored. This process is reversible, allowing the sensor to be used repeatedly for NH$_3$ detection.

4.5. Gas Sensing with PANI/Metal Oxide Nanomaterials

Metal oxides generally have good gas-sensing properties, but they require high operating temperatures. When combined with PANI, the nanocomposite sensor's performance can be significantly enhanced due to the formation of a p-n junction between the metal oxides and PANI. In a study by Qu et al., the researchers explored the synthesis and characterization of double-shell hierarchical SnO$_2$@PANI (DSP) composites for NH$_3$ gas sensing at room temperature [93]. The synthesis involved a hydrothermal method to produce carbon microspheres, which acted as templates for forming D-SnO$_2$ microspheres. These were subsequently coated with PANI through in situ oxidative polymerization. The authors modulated the molar ratios of D-SnO$_2$ and aniline (n_D-SnO$_2$: n_aniline × 100% = 0%, 10%, 20%, 30%, and 60%), where x represents the D-SnO$_2$ molar content in DSPx. The composites were then deposited onto PET substrates to create flexible, electrode-free sensors [82]. TEM images showed that D-SnO$_2$ had a hierarchical double-shell spherical structure, while DSP20 retained this morphology with PANI forming a conductive network on the surface. The DSP20 sensor had a significantly higher response to NH$_3$ compared with pure PANI, with a response value of 37.92 for 100 ppm NH$_3$, which is 5.1 times greater than that of the pristine PANI sensor. The DSP20 sensor also showed excellent selectivity and repeatability. At a lower concentration of 10 ppm NH$_3$, the sensor's response and recovery times were 182 s and 86 s, respectively, indicating the rapid response and recovery capabilities of the sensor. The authors also found that increasing relative humidity from 20% to 56% enhanced the sensor's response to NH$_3$, but a further increase in RH degraded performance. The stability tests over 17 days showed that the response to 10 ppm NH$_3$ dropped about 50% by the third day, stabilizing thereafter. This improved sensing performance was attributed

to the unique microstructure and the formation of p-n heterojunctions between PANI and D-SnO$_2$, which enhanced electron transfer [93].

Dhanawade et al. synthesized a PANI-CeO$_2$ nanohybrid for NH$_3$ detection at room temperature using a facile chemical oxidative polymerization process [94]. TEM images revealed a uniform distribution of CeO$_2$ nanoparticles within the PANI matrix, forming a highly interconnected nanofiber structure. The PANI-CeO$_2$ (50 wt%) nanohybrid sensor had a notable 80% response to 100 ppm NH$_3$, significantly outperforming pristine PANI, which showed a 26.70% response. The sensor's dynamic response to varying NH$_3$ concentrations showed high sensitivity and good reaction times at room temperature. It also featured a rapid response time of 9.31 s and a recovery time of 531.60 s when exposed to 100 ppm NH$_3$. The gas-sensing mechanism involved NH$_3$ interacting with the PANI-CeO$_2$ surface, causing an increased resistance due to NH$_4^+$ ion formation. Impedance spectroscopy was used to explore this interaction mechanism. The sensor's stability over 40 days showed outstanding selectivity and stability of 78.75%, demonstrating long-term reliability at 25 °C. Additionally, the sensor could detect NH$_3$ at concentrations as low as 10 ppm, showcasing its potential for monitoring biomarker NH$_3$ at 25 °C [94].

Zhang et al. designed flexible hydrogen sulfide (H$_2$S) gas sensors using PANI and copper oxide nanoparticles (CuO NPs) [95]. The PANI/CuO nanocomposites were synthesized using in situ polymerization (P-1) and bilayer (P-2) methods. The diameter of the PANI fibers was 170 nm, while the CuO NPs were around 80 nm in size. It was found that the P-2 composite exhibited a more uniform distribution of CuO on the PANI fibers in comparison with the P-1 composite. The sensor developed using the P-2 method demonstrated a high sensitivity of 7.25 compared with 2.16 for the P-1 method and excellent responsiveness ($\Delta R = 188\%$) for H$_2$S concentrations ranging from 0 to 25 ppm in ambient conditions. Moreover, the PANI/CuO (P-2) composite sensor displayed high sensitivity to H$_2$S at 25% and NH$_3$ at 8%, indicating excellent selectivity for H$_2$S in ambient conditions. This sensor also demonstrated good stability and flexibility after 60 and 120 bending cycles, making it suitable for detecting H$_2$S in fresh food packaging, particularly meat, as an indicator of spoilage [95].

When an In$_2$O$_3$-PANI (indium oxide on PANI) sensor is exposed to methanol vapor, the methanol molecules initially adsorb onto the sensor's surface through both physical and chemical interactions (see Figure 20) [96]. The In$_2$O$_3$ NPs provide active sites for this adsorption and accelerate the oxidation of methanol vapor, facilitating the transfer of electrons to the PANI matrix. This electron transfer lowers the number of charge carriers in the PANI, which increases the sensor's resistance and decreases its conductivity. This change in conductivity acts as a measurable signal indicating the presence of methanol vapor. Additionally, the adsorption of methanol causes the PANI matrix to swell, which increases the distance between conductive pathways within the nanocomposite and further decreases conductivity. In terms of band energy diagrams, in the presence of methanol gas, the electron donation from methanol to the sensor increases the depletion region, reducing the number of holes, and thus, decreasing conductivity [97]. When the sensor is exposed to air, the methanol molecules desorb, the depletion region decreases, and the sensor regains its original conductivity as the holes in the PANI matrix are restored. The presence of a p-n junction between indium oxide (n-type) and PANI (p-type) further enhances this effect. The p-n junction creates a built-in electric field that facilitates the separation of charge carriers, improving the sensor's sensitivity and response time [97]. This reversible process allows the sensor to be used repeatedly for methanol detection.
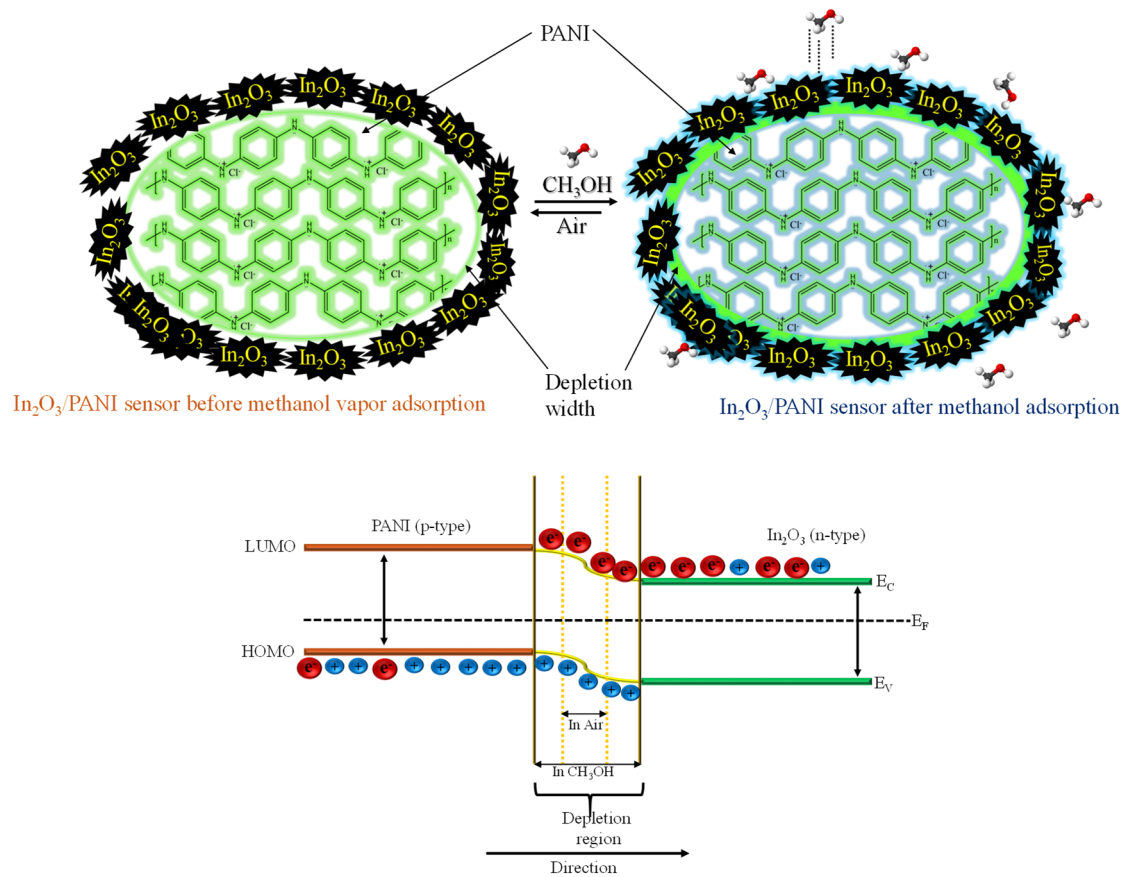
Figure 20. Schematic illustration of In$_2$O$_3$-PANI and band structure with and without adsorbed gas analyte. The image is not drawn to scale.

Pal et al. conducted a study on the synthesis and application of polyaniline/vanadium pentoxide (PANI/V$_2$O$_5$) nanocomposites for the selective detection of methanol at room temperature [98]. The composites were synthesized by integrating various concentrations of V$_2$O$_5$ (V1~5%, V2~10%, V3~20%, and V4~30% by weight) into the PANI matrix through oxidative polymerization. The FE-SEM images revealed spherical V$_2$O$_5$ nanoparticles with sizes ranging from 80 to 90 nm, and the PANI/V$_2$O$_5$ composites exhibited agglomerated structures with reduced particle sizes attributed to the presence of V$_2$O$_5$. The study found that increasing the concentration of V$_2$O$_5$ in PANI significantly enhanced the sensing response of the fabricated devices to methanol vapor. Specifically, the methanol sensor (30% V$_2$O$_5$ in PANI) demonstrated a notable sensing response of approximately 36% at a concentration of 60 ppm. This composite sensor showed a response time of 120 s and a recovery time of 330 s, with a limit of detection (LOD) of 0.051. The response of pure V$_2$O$_5$ NPs to methanol vapor increased at higher temperatures (100 °C, 150 °C, and 200 °C), while minimal sensitivity to other gases such as carbon dioxide, hexane, chloroform, and acetone was observed at room temperature when compared with methanol. Moreover, the fabricated devices were tested in various chemical environments. The V4 composite sensor exhibited sensitivities of approximately 2.96% for CO$_2$, 3.51% for hexane, 5.25% for chloroform, 8.14% for acetone, 34.23% for ethanol, and 46.91% for methanol, with the highest sensitivity observed for methanol. The sensing mechanism was attributed to the interaction between methanol molecules and the PANI/V$_2$O$_5$ interface, resulting in carrier concentration and mobility changes and thereby affecting the sensor's resistance [98].

Kaur et al. explored the synthesis and characterization of PANI and its nanocomposite with zinc oxide (ZnO) for enhanced NH$_3$ sensing at room temperature [97]. Various samples with different ZnO weight percentages (5 wt%, 10 wt%, 20 wt%, 30 wt%, 40 wt%, and

50 wt%) were incorporated into the PANI matrix and labeled PZ5, PZ10, PZ20, PZ30, PZ40, and PZ50, respectively. These samples were then examined for NH_3 sensing properties across a temperature range of 20–100 °C. The synthesis of PANI nanofibers was carried out through a chemical oxidative polymerization process, while the preparation of ZnO nanoplates involved utilizing a cetyltrimethylammonium bromide (CTAB)-assisted hydrothermal method. The synthesized powders were applied to aluminum interdigitated electrodes using the doctor blade method. PANI–ZnO nanocomposite sensors were then fabricated. The SEM image revealed a nanoplate-like structure for ZnO and thick fiber-like morphologies for PANI, with ZnO well dispersed in the PANI matrix. Gas-sensing measurements demonstrated that the sensor's response decreased with increasing temperature, with the PZ20 sample showing the highest response at room temperature. The PZ20 sensor exhibited a notable response of 16.95% to 100 ppm NH_3 at room temperature, a low detection limit of 5 ppm, and response/recovery times of 18/87 s. In comparison, pure PANI showed a response of 9.31% and response/recovery times of 39/103 s for the same NH_3 concentration. The composite sensor also showed reliable repeatability, long-term durability, and selectivity, specifically toward NH_3, compared with gases like H_2, C_2H_5OH, NO_2, CO, and CO_2. The sensing mechanism involved a p-n heterojunction between PANI and ZnO, forming a depletion region at the interface. The authors suggested that introducing a reducing gas such as NH_3 widens the depletion layer and disrupts the electric field [97]. On the other hand, exposure to an oxidizing gas such as NO_2 reduces the depletion width by removing electrons, also disrupting the electric field. These modifications at the interface change the electrical conductivity, enhancing the sensor's response.

4.6. Gas Sensing with PANI/Metal Chalcogenide Nanomaterials

Combining PANI with metal chalcogenides (compounds of a metal and elements like sulfur, selenium, or tellurium) can result in nanocomposites with enhanced gas-sensing properties. Transition metal dichalcogenides (TMDs) are being explored for gas sensing due to their high room-temperature sensitivity, which can be further improved by forming heterostructures with PANI. In a study conducted by Fadojutimi et al., a nanocomposite comprising PANI and zirconium disulfide (ZrS_2) was developed for sensing primary alcohols at room temperature [99]. PANI was produced through chemical polymerization, while ZrS_2 was exfoliated using a sonication process. The TEM analysis revealed the presence of layered nanosheets of both PANI and ZrS_2, with ZrS_2 appearing as dark stains within the PANI matrix. The sensor's response and recovery curves to isopropanol vapor (58–289 ppm) and 45% RH exhibited a distinct signal with minimal noise and demonstrated response and recovery times of 58 s and 88 s, respectively. The authors calculated the sensitivities of the PANI-ZrS_2 sensors to methanol, ethanol, and isopropanol from the slopes of their respective linear fitted graphs as 43%, 58%, and 104%, respectively. Moreover, the sensor's response to methanol and ethanol vapors exhibited variations under different humidity conditions, with a transition from p-type to n-type behavior observed at elevated humidity levels, particularly at 64% for methanol and 75% for ethanol [99].

Feng et al. investigated the synthesis and application of PANI/WS_2 nanocomposites for flexible NH_3 gas sensors at room temperature [100]. The nanocomposites were synthesized using in situ polymerization, and the addition of WS_2 was at mass fractions of 2, 4, and 6 wt%, which were denoted as PANI/WS_2-2, PANI/WS_2-4, and PANI/WS_2-6, respectively. The prepared PANI exhibited a porous, interconnected branched structure, while the WS_2 displayed a lamellar 2D structure. The PANI/WS_2 composite formed a heterojunction structure, combining the branched PANI with the lamellar WS_2. From the gas-sensing results of the PANI/WS_2 composites, the sensor's peak resistance increased with the addition of WS_2, with the best performance observed at a 2% WS_2 mass fraction.

The addition of layered WS_2 to form a heterojunction structure with PANI increased the carrier transport rate and improved gas-sensing performance. However, excessive WS_2 resulted in incomplete coverage of WS_2 by PANI, which led to NH_3 absorption by WS_2 and decreased gas-sensing performance. It was also demonstrated that excessive WS_2 thickened the heterojunction depletion layer between the PANI and WS_2, further reducing sensing performance. The PANI/WS_2-2 sensor improved performance by 1.33 times (at 20 ppm) compared with the pure PANI sensor toward NH_3. The composite sensor demonstrated a higher sensitivity of 34.04% ppm^{-1} to NH_3 at various concentrations compared with 30.94% ppm^{-1} for the pure PANI sensor. The PANI/WS_2-2 sensor showed an 8% response to 100 ppb with a response time of 108 s and a recovery time of 229 s, which was 43 s faster than pure PANI. The sensor also maintained a stable performance over 30 days and demonstrated improved selectivity to NH_3 over other gases. The PANI/WS_2-2 sensor's cross-sensitivity in the presence of the interfering gases C_2H_5OH, $(CH_2OH)_2$, C_6H_{14}, C_3H_8O, and CH_3COCH_3 (all at 5 ppm) revealed a greater response to NH_3. This enhanced selectivity was ascribed to the addition of WS_2, making the sensor promising for NH_3 monitoring [100].

Chen et al. synthesized $MoTe_2$/PANI nanocomposites using in situ chemical oxidation polymerization, which were then used to manufacture NH_3 gas sensors with an IDE transducer [101]. The HRTEM analysis revealed PANI nanofibers surrounding the lamellar $MoTe_2$ nanosheets, creating a porous mesh microstructure. This enhanced the surface area of the PANI layers, providing more active sites for gas molecule adsorption. The $MoTe_2$/PANI composite sensors showed a markedly higher response to NH_3 gas within the 10–1000 ppm concentration range (at $62.7 \pm 3\%$ RH and $22 \pm 2\,^\circ$C) compared with pure PANI sensors. The 8 wt% $MoTe_2$/PANI composite sensor demonstrated the most significant response, being 4.23 times more responsive than the pure PANI sensor at 1000 ppm NH_3 gas. Additionally, the response and recovery times indicated that the 8 wt% $MoTe_2$/PANI sensor had faster response (25 s) and recovery (24 s) times compared with the pure PANI sensors. The sensor consistently responded over repeated cycles and displayed high selectivity toward NH_3 over other gases such as CH_4, C_2H_5OH, and NO_2. The mechanism behind the enhanced NH_3 sensitivity in the $MoTe_2$/PANI composites was influenced by the energy levels of the materials. PANI had a band gap of 2.8 eV, while 2H-$MoTe_2$ had a band gap of 1.0 eV. Therefore, when PANI nanofibers underwent polymerization on 2H-$MoTe_2$ nanosheets, the change in carrier concentrations led to the migration of holes in PANI and electrons in 2H-$MoTe_2$ until an equilibrium state was achieved, resulting in the formation of p-n heterojunctions. Exposure to NH_3 gas led to NH_3 molecules capturing more protons (H^+) from the composites, reducing PANI doping concentrations, increasing its resistance, and broadening the depletion layer of the p-n heterojunction, thereby enhancing the NH_3 gas-sensitive response [101].

Ghaleghafi and Rahmani investigated the development of MoS_2/PANI nanocomposites for room-temperature NH_3 sensing [102]. The researchers synthesized these nanocomposites using a hydrothermal method with varying amounts of PANI. The TEM image showed 1D-PANI nanofibers enveloped by 2D MoS_2 nanosheets, resulting in a porous architecture that significantly enhanced gas-sensing performance. Their findings showed the dynamic response of the MoS_2/PANI (1:1) sensor to varying NH_3 concentrations (10–100 ppm) with a strong and stable response of 1.44% at 100 ppm and LOD of 10 ppm. The sensor exhibited a linear relationship between gas response and NH_3 concentration, with a high sensitivity of approximately 0.0153% per ppm and a correlation coefficient of 0.99. The MoS_2/PANI sensor also demonstrated faster response/recovery times of 54/49 s, highlighting its exceptional capability for achieving precise and reliable detection of NH_3

vapor at room temperature [102]. Moreover, the sensor exhibited consistent performance with less than 5% variation over multiple cycles.

When the Ni_3Te_2-PANI sensor is exposed to ethanol vapor, the ethanol molecules initially adhere to the sensor surface through both weak physical forces and stronger chemical interactions (Figure 21) [103]. The Ni_3Te_2 nanoparticles provide active sites for ethanol adsorption and oxidation, facilitating the transfer of electrons from the ethanol molecules to the Ni_3Te_2-PANI sensor. This electron transfer decreases the concentration of charge carriers (holes) in the PANI matrix, resulting in increased resistance and reduced conductivity, which generates a measurable signal indicating the presence of ethanol vapor. The p-n junction between Ni_3Te_2 (n-type) and PANI (p-type) further enhances the sensor's performance by establishing an internal electric field that aids in separating charge carriers, thereby improving sensitivity and response time. In terms of energy band diagrams, the electron donation from ethanol increases the depletion region, reducing the number of holes and thus lowering conductivity. When the sensor is exposed to air, the ethanol molecules detach, the depletion region shrinks, and the sensor's original conductivity is restored as the holes in the PANI matrix are replenished. Additionally, ethanol adsorption can cause the PANI matrix to swell, increasing the spacing between conductive pathways in the nanocomposite, which further reduces conductivity. This swelling effect enhances the separation of conductive paths, amplifying the drop in conductivity.
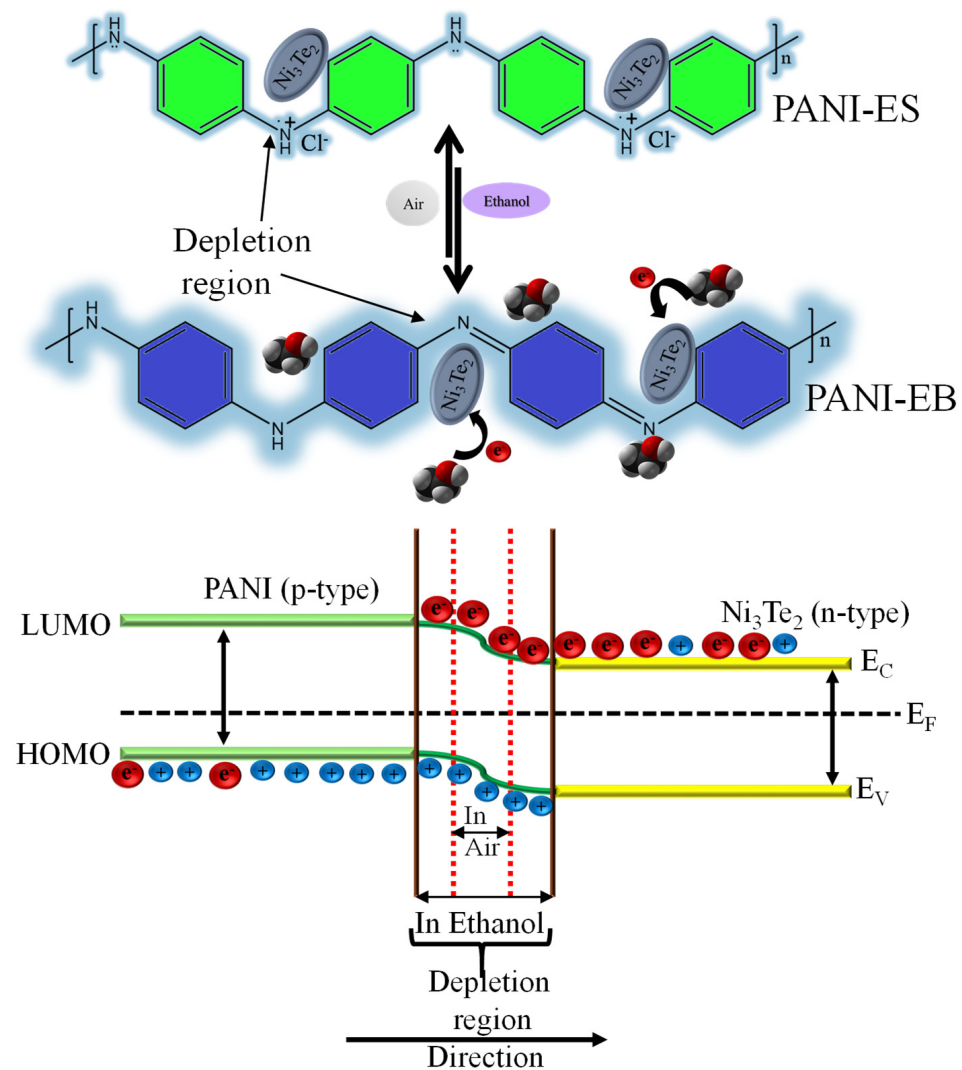
Figure 21. Graphical illustration of Ni_3Te_2-PANI sensing mechanism to ethanol gas and band structure at the p-n interface. The figure is not drawn to scale.

4.7. Gas Sensing with Ternary PANI Nanocomposites

Qiu et al. synthesized a $PANI/CoMoO_4$ heterogeneous nanocomposite via in situ polymerization of highly active PANI onto $CoMoO_4$ [104]. TEM analysis showed that the $CoMoO_4$ nanorods were uniformly coated with PANI nanosheets, creating a rough surface suitable for gas adsorption. The composite's exceptional performance demonstrated a significantly higher response to NH_3 than pure PANI, excellent cyclic stability with less than 2% error in repeated tests, and effective detection capabilities under varying humidity levels. The real-time dynamic resistance response of PANI nanosheets and the $PANI/CoMoO_4$ composite to NH_3 was investigated within a concentration range of $0.05-50$ ppm at standard room temperature (25 ± 2 °C) and 15 ± 2% RH. The data indicated the superior intensity of $PANI/CoMoO_4$ response to different concentrations of NH_3 compared with the PANI sensor. The composite sensor showed a practical detection limit with a very low LOD of 50 ppb for NH_3. The calibration curve showed that the response of the $PANI/CoMoO_4$ sensor was directly proportional to the NH_3 concentration across the tested range, as demonstrated by a strong linear regression ($R^2 = 0.993$) between 1 and 50 ppm. Additionally, the response time of $PANI/CoMoO_4$ to NH_3 was approximately 5 s, significantly shorter than that of PANI. Repeatability tests to 5 on/off cycles under 50 ppm concentrations of NH_3 demonstrated a remarkably low error rate of less than 2%, indicating the robust cyclic stability of $PANI/CoMoO_4$ in the presence of NH_3 gas. The response of $PANI/CoMoO_4$ to 50 ppm NH_3 at varying RH levels from 10% to 90% showed that an increase in humidity initially resulted in a higher response of $PANI/CoMoO_4$ to NH_3, followed by a subsequent decrease at higher humidity levels. This behavior was attributed to two primary factors: the influence of humidity on the wettability of the $PANI/CoMoO_4$ surface, impacting its adsorption characteristics, and the competitive adsorption of water molecules at higher humidity levels, affecting the response to NH_3 [104].

In a recent study, Masemola et al. investigated the complex production process of NGQDs/PANI/PAN composite fibers, which were specifically designed for alcohol sensing at ambient temperatures [105]. The researchers employed a microwave-assisted hydrothermal method to synthesize the NGQDs, seamlessly integrating them into the PANI through in situ polymerization. Subsequently, composite nanofibers were crafted using electrospinning with polyacrylonitrile (PAN). As a result, the NGQDs/PANI/PAN fibers, exhibiting a rough surface and an average diameter of 489 ± 21 nm, showed a substantial maximum response of 3.7% to 100 ppm of ethanol, showcasing a notable increase when compared with NGQDs/PANI and PANI sensors (Figure 22a). This performance was attributed to the increased surface-to-volume ratio of the fibers due to the concentration of oxygen functional groups, active sites, defects, and vacancies on the fiber surface, thus facilitating the adsorption and diffusion of ethanol vapor. The dynamic response curves of the sensor to 100 ppm of methanol, ethanol, and isopropanol vapors were 1.29%, 3.66%, and 4.60%, respectively, at room temperature and 45% RH (Figure 22b). Additionally, the corresponding response and recovery times for methanol, ethanol, and isopropanol were 127/113 s, 64/57 s, and 99/88 s, respectively. The NGQDs/PANI/PAN sensor also demonstrated sensitivities of 0.03, 0.02, and 0.031% ppm^{-1} toward methanol, ethanol, and isopropanol vapors, respectively. Notably, the sensor's stability and practical suitability were highlighted by its repeatability over four cycles for 100 ppm of all the tested alcohols [105].
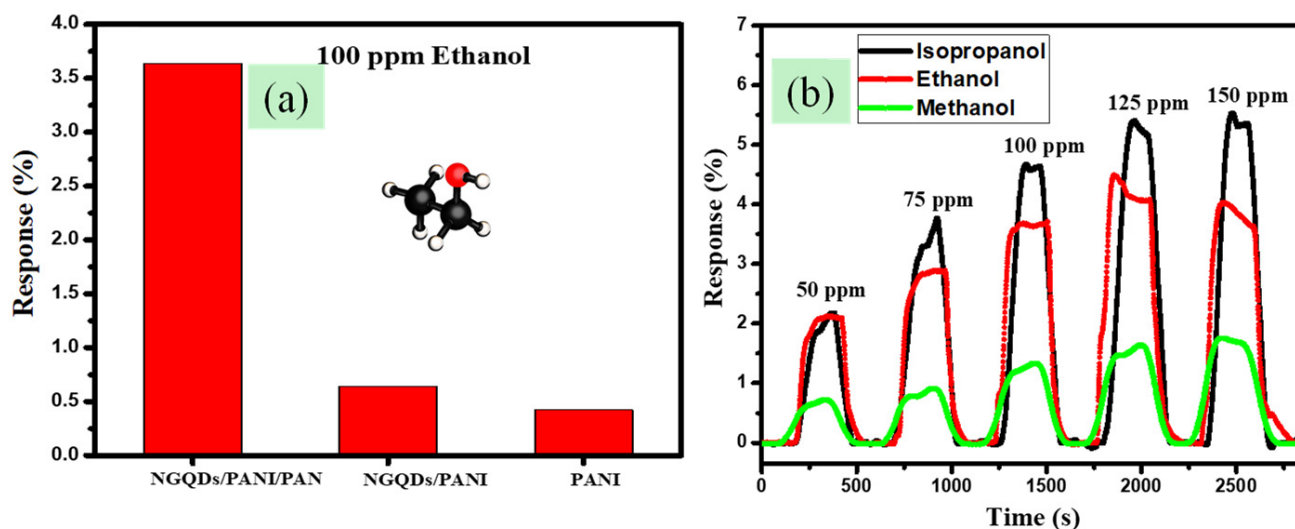
Figure 22. 1 Gas response (%) of a NGQDs/PANI/PAN sensor toward 100 ppm of methanol, ethanol, and isopropanol (RH 45%) (**a,b**). Reprinted with permission from [105], copyright 2024 IEEE.

Rahim and colleagues performed a study on the synthesis and characterization of a highly sensitive room-temperature NH_3 sensor utilizing PANI/bismuth-doped zinc oxide (PANI/Bi-ZnO) composites [106]. The synthesis process involved the use of inverse emulsion polymerization to coat the PANI/Bi-ZnO on a substrate with staggered electrodes, thus creating the sensor. The SEM analysis indicated that pure PANI had a uniform membrane-like morphology, while PANI/Bi-ZnO exhibited a non-uniform dispersion of metallic traces within the polymer matrix, signifying the presence of Bi-ZnO. The PANI/Bi-ZnO sensor displayed a linear increase in sensitivity with rising NH_3 concentrations, achieving a sensitivity of 410% at 70 ppm. This exceptional sensitivity of the PANI/Bi-ZnO sensor was attributed to the formation of p-n heterojunctions, which enhanced the charge transfer process, resulting in a high response and recovery time of 11/15 s at 20 ppm NH_3. The selectivity tests revealed that the sensor selectively responded to NH_3 in comparison with other organic vapors. Moreover, the sensor demonstrated repeatability and stability over multiple cycles, with a quick recovery of the sensing signal, indicating a weak bonding between NH_3 molecules and the sensor surface. The LOD was determined to be 20 ppm. According to the report, when PANI (p-type) encounters a reducing gas such as NH_3, it undergoes reduction, leading to an increase in sample resistance due to a reduction in charge carriers. Combining PANI with n-type Bi-ZnO created p-n heterojunctions, forming an electron donor and acceptor system that affected charge transport in the composite. Consequently, PANI/Bi-ZnO exhibited higher gas sensitivity than the pure counterparts. The response of the composite to NH_3 increased in a similar manner to that of pure PANI, and this indicated that potential competing mechanisms within the composite existed, with PANI playing a dominant role [106].

Mathe et al. recently reported on the use of a PANI/In$_2$O$_3$/OLCs composite for NH$_3$ sensing at room temperature [107]. In this work, the authors reported on the use of In$_2$O$_3$ nanoparticles that were synthesized using different microwave-assisted hydrothermal methods. The prepared samples both showed enhanced responses toward NH$_3$ when compared with bare PANI, with the annealed In$_2$O$_3$ showing a higher response while the rod-like In$_2$O$_3$ showed a more linear response to NH$_3$ in the measured range of concentration [107].

Exposing a reduced graphene oxide-Ag nanoparticle-PANI (rGO-Ag/PANI) sensor to H$_2$S gas initiates the adsorption of the gas molecules onto the sensor's surface through both weak physical forces and stronger chemical interactions (Figure 23) [108]. The rGO is particularly effective due to its high surface area, which allows for a greater number of adsorption sites, and its excellent electrical conductivity, which facilitates efficient electron transfer. Ag NPs enhance the catalytic activity and improve the sensor's sensitivity by providing additional active sites and facilitating the oxidation of H$_2$S at room temperature. PANI serves as the matrix that supports both the Ag nanoparticles and rGO, providing a conductive pathway for electron flow. In the presence of H$_2$S molecules, Ag nanoparticles oxidize the H$_2$S into H$^+$ and HS species; the concentration of HS species will balance some of the charged N$^+$ species on the PANI backbone, and some will form Ag-S, releasing highly mobile H$^+$ ions and decreasing the resistance of the rGO-Ag/PANI sensor [109]. This change in conductivity serves as a measurable signal indicating the presence of H$_2$S gas. When the sensor is exposed to air, the H$_2$S molecules desorb and the sensor's original conductivity is restored as the concentration of mobile H$^+$ ions and HSdecrease in the PANI matrix. The combined action of rGO and silver nanoparticles supported on the conductive PANI at room temperature significantly enhances the sensor's performance, allowing for effective and repeated detection of H$_2$S gas [109]. Additional recent works on PANI-based nanocomposite sensors are summarized in Table 3.
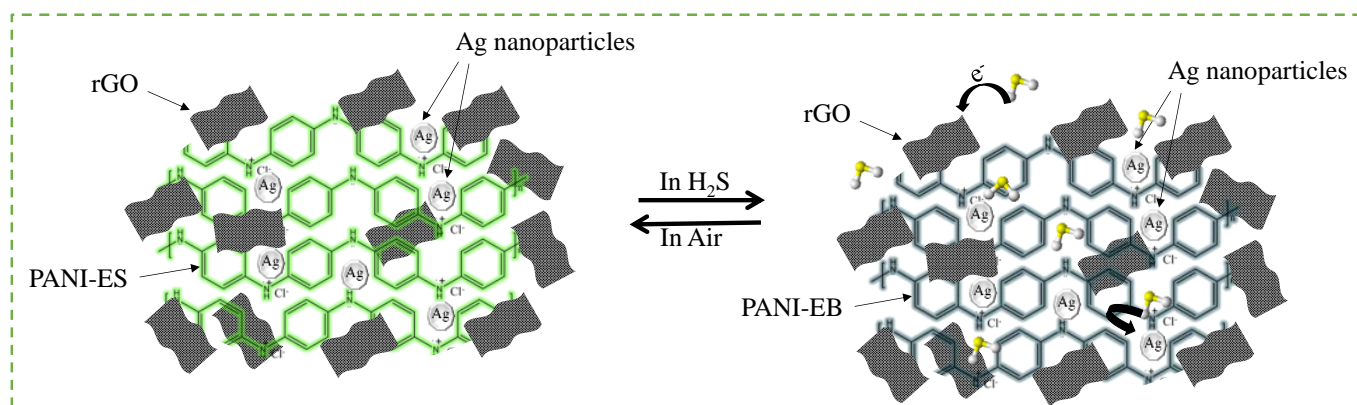
Figure 23. H$_2$S gas sensing mechanism of ternary rGO-Ag/PANI sensor. The figure is not drawn to scale.

Table 3. Reported data on different PANI-based nanocomposite sensors.

Sensing Material	Gas Analyte	Response/Concentration	$t_{response}$	$t_{recovery}$	LOD $^\$$	W_T *	Remarks	Reference
Cu-en/PANI	NH$_3$	3.8% (100 ppm)	100 s	50 s	2 ppm	RT ^	Improved selectivity	[110]
Au/PANI/WS$_2$	NH$_3$	286.1% (100 ppm)	24 s	26 s	13.8 ppb	RT	Fast response/recovery times and large response	[111]
Cu-rGO/PANI	Methanol	64.22% (500 ppm)	30 s	45 s	-	RT	Increased conductivity and sensitivity	[112]
PANI-Sr	NH$_3$	498% (100 ppm)	1 s (50 ppm)	42 s (50 ppm)	0.013 ppm	RT	Quick response/recovery times	[113]
Au-PANI-TiO$_2$	NH$_3$	123% (100 ppm)	32 s	111 s	-	-	Improved response	[114]
GP-PANI@RT	NH$_3$	60% (1 ppm)	46 s	198	100 ppb	RT	Enhanced sensor flexibility	[115]
PVA/WPPy/V$_2$O$_5$	LPG	1.16% (600 ppm)	10 s	8 s	-	RT	Excellent selectivity, sensitivity, and stability	[116]
AgCl@PA-PANI/GO	CO	19.5% (130 ppm)	50 s	39 S	-	RT	Enhanced sensitivity and shortened response/recovery time.	[117]
PANI/AC	Methanol	43% (200 ppm)	25 s	305 s	<1 ppm	RT	Enhanced stability and selectivity	[118]
Ce–ZnO/PANI	LPG	80% (100 ppm)	157 s	154 s	<30 ppm	RT	Enhanced response to LGP	[119]
PANI-CdS	NH$_3$	250% (100 ppm)	58 s	104 s	14 ppm	RT	Excellent selectivity	[120]
Pt/MoS$_2$/PANI	NH$_3$	16.64% (50 ppm)	15 s	103 s	250 ppb	RT	Improved flexible sensor stability	[121]
Ag-ZnO/Pani	NH$_3$	50% (50 ppm)	23 s	58 s	<5 ppm	RT	Improved selectivity, response/recovery times	[122]
Au$_{15}$Ag$_{15}$@GO/PANI	NO$_2$	50% (50 ppm)	431 s	296 s	0.3	RT	Quick response/recovery times	[123]
PANI/NiO-loaded TiO$_2$	Acetone	1030% (50 ppm)	150 s	290 s	175.2 ppb	RT	Excellent long-term stability	[124]
Cu-PANI-MoO$_3$	NH$_3$	17.11% (100 ppm)	41 s	179 s	20 ppb	RT	Outstanding response/recovery times, repeatability, and selectivity	[125]
(Cu–S)$_n$ MOF/PANI	H$_2$S	21.68% (30 ppm)	15 s	1155 s	0.5 ppm	RT	Enhanced conductivity and sensor performance	[126]
PANI/Ag$_2$O	CO	97% (100 ppm)	37 s	41 s	2 ppm	RT	Improved stability (60 days)	[127]
V$_2$CT$_x$@PANI	NH$_3$	155.78% (100 ppm)	22 s (15 ppm)	15 s (15 ppm)	5 ppm	RT	Improved long-term stability and selectivity	[128]
PANI)/black phosphorus (BP)	NO$_2$	2204% (60 ppm)	98 s	406 s	2 ppm	RT	Improved response and drift issues	[129]

* W_T—Working temperature; ^ RT—Room temperature; $^\$$ LOD—Limit of detection.

5. Key Suggestions to Consider for Overcoming the Limitations of PANI-Based Chemiresistors

The field of PANI nanocomposite chemiresistors at room temperature presents several current challenges that require innovative solutions and offer exciting perspectives for future research. One significant challenge lies in the synthesis and characterization of materials. Developing soluble PANI derivatives is crucial for enhancing processability and ensuring uniform sensor films, which are essential for consistent performance. Increasing the surface area of the PANI nanostructures can improve sensitivity, however, it is vital to determine the optimal surface area. To improve sensitivity, researchers must focus on controlling the morphology and increasing the surface area using composites like carbon nanomaterials and metal oxides. Environmental stability is another critical area of concern. PANI sensors often exhibit diminished sensitivity under high-temperature and high-humidity conditions. Addressing this issue is essential for achieving stable sensor performance in complex environmental settings. Including fluorinated groups and hydrophobic matrices can minimize water uptake, promoting stable sensor performance in varying humidity conditions.

Broadening the gas detection capabilities of PANI sensors is also imperative. While these sensors are highly sensitive to NH_3, their sensitivity to other gases, such as CO, NO_2, and H_2S, is significantly lower. Enhancing the sensitivity of PANI composites to a broader range of gases can expand their application scope, making them more versatile. Researchers should focus on using metal oxides, nanoparticles, and tailored dopants to provide specific binding sites for target gases, thereby enhancing selectivity and improving sensor performance. The detection of VOCs by PANI nanocomposite chemiresistors is another area that requires further exploration to improve their applicability in various industrial and environmental settings. The long-term performance and stability of PANI chemiresistors is another area of concern. Research must focus on addressing issues related to sensor degradation over time, including reduced repeatability and natural performance degradation. Incorporating stable nanomaterials and forming robust composite structures can address the inherent instability of pure PANI, enhancing the long-term sensor durability. Ensuring uniform composite structures and stable chemical modifications can provide consistent performance across multiple sensing cycles, improving repeatability and reproducibility. Integration with other technologies offers promising solutions to enhance the functionality of PANI sensors. Combining PANI sensors with other types of sensors such as stress, temperature, and proximity sensors can create comprehensive monitoring systems that provide detailed environmental data. Moreover, integrating PANI sensors with energy devices for self-powering and wireless signal transmission can significantly improve their practicality and ease of use. Introducing conductive fillers can also improve electron transfer and provide more active gas adsorption/desorption sites, reducing response and recovery times for improved performance.

Advancements in materials and fabrication techniques hold great potential for the future of PANI sensors. Exploring hybrid nanomaterials, such as combining PANI with graphene or transition metal dichalcogenides, can enhance sensitivity and selectivity, enabling the detection of a broader range of gases, including VOCs and other industrial hazards. Functionalizing PANI with different groups can further tailor its properties for specific gas detection applications. Advanced 2D materials, such as functionalized polymers, transition metal dichalcogenides, hybrid nanomaterials, graphene, and ternary composites, offer exceptional sensitivity and selectivity, promising the detection of a broader spectrum of gases. The electrical conductivity of PANI can be easily manipulated through doping or reduction processes, resulting in either conductive or non-conductive states. The level of conductivity in PANI is influenced by the type and amount of dopant used,

as these dopants generate charge carriers responsible for electrical conductivity. This fundamental chemical property makes PANI highly suitable for vapor and gas detection. PANI-based sensors are generally known for their high sensitivity and rapid response times, especially at ambient temperatures. However, they face challenges, such as poor stability, limited surface area, low sensitivity at room temperature, and relatively lower conductivity compared with metal conductors. To address these issues, creating nanocomposites of PANI with metal oxides (such as WO_3, In_2O_3, SnO_2), metals (like Cu, Au, Ag, Zn), and functionalized carbon-based materials (such as carbon dots, CNTs, HCS, and graphene) is expected to significantly enhance the gas-sensing properties and improve performance at room temperature. Finally, developing cost-effective fabrication techniques is vital for the widespread adoption of PANI sensors. Research should focus on scalable methods that maintain sensor performance while reducing production costs, making these sensors accessible to various industries. The future of PANI chemiresistor nanocomposite sensors is promising, with numerous opportunities for innovation. By addressing these challenges and exploring new solutions, researchers can develop more sensitive, selective, and stable sensors that meet the demands of diverse applications, from environmental monitoring to healthcare. The integration of advanced materials and technologies will undoubtedly drive the next generation of gas sensors, contributing to safer and healthier environments.

6. Future Guidelines for Designing High-Performing Chemiresistor Devices Based on PANI Composites and Their Relevance

The development of PANI-based chemiresistors offers considerable potential to support multiple SDGs by improving air quality monitoring, enhancing public health, and promoting sustainable industrial practices. Future research should focus on the following strategies to overcome the current limitations and advance the performance of these sensors:

Optimization of nanocomposite structures: Future research should focus on optimizing nanocomposite structures by selecting dopants and secondary materials that enhance surface area, gas adsorption capabilities, and electrical conductivity. For example, the integration of graphitic carbon nitride (g-C_3N_4) with PANI has been shown to improve sensitivity to NH_3 due to increased specific surface area and effective dispersion of PANI in the composite structure. The use of materials like metal–organic frameworks (MOFs) or graphene derivatives could further enhance gas interactions, supporting SDG 9 by advancing sustainable technologies in industrial applications.

Functionalization and doping: Exploring various dopants and functional groups that specifically interact with target gases can enhance sensitivity and selectivity. For example, doping PANI with serine (an amino acid) resulted in petal-like nanostructures that significantly increased the surface area and improved NH_3 sensitivity due to enhanced interaction with gas molecules. This strategy promotes SDG 12 by enabling the use of more effective and targeted dopants.

Morphology control: Controlling the morphology of PANI composites is crucial for enhancing gas-sensing performance. For instance, PANI/PVA hydrogels developed through repetitive freeze–thaw cycles achieved a 3D porous structure that facilitated efficient gas absorption and desorption, leading to improved sensitivity and response times. Techniques like electrospinning, self-assembly, and templating could be refined to achieve such morphologies.

Hybrid composites: Combining multiple materials (e.g., metal oxides, carbon nanomaterials, and metal nanoparticles) in a single composite can synergistically enhance gas-sensing properties. For example, PANI-ZnO nanocomposites have demonstrated enhanced sensitivities and response times in NH_3 detection due to the increased surface

area and active sites provided by ZnO. Similarly, PANI-Ag nanocomposites showed ultra-sensitivity to NH_3 due to the synergistic effects of silver nanoparticles. These approaches contribute to SDG 7 by providing efficient and low-cost sensors.

Advanced fabrication techniques: Utilizing advanced fabrication techniques like 3D printing, layer-by-layer assembly, and atomic layer deposition can achieve precise control over the thickness, uniformity, and structure of sensing materials. These methods were demonstrated in the creation of fluorinated PANI-based sensors that showed improved NH_3 sensitivity due to their precise structural properties. Advanced fabrication techniques support SDG 9 by enabling scalable and reproducible manufacturing processes.

Environmental stability and selectivity: Addressing the environmental stability of PANI composites, particularly their performance under varying humidity and temperature conditions, is critical. For example, fluorinated PANI-based sensors demonstrated enhanced stability by reducing water uptake, while PSS-doped PANI on PVDF membranes minimized the effects of humidity by maintaining a stable matrix.

Integration with flexible electronics: Developing flexible and wearable sensors by integrating PANI composites with flexible substrates (such as polyimide or polyethylene terephthalate) could expand applications in health monitoring and wearable electronics. For example, PSS-PANI/PVDF composites demonstrated flexibility and high sensitivity, suitable for real-time monitoring of air pollutants and health indicators. This aligns with SDG 3 by promoting innovative technologies for health and environmental monitoring.

Develop eco-friendly PANI composites: Fabricating PANI composites using environmentally benign methods, such as green solvents, natural dopants, and sustainable precursors, is essential. This approach was exemplified by using amino acids like serine as dopants to enhance gas sensor performance in a more sustainable manner. It contributes to SDG 12 by reducing hazardous waste and promoting cleaner production processes.

Enhance sensor durability and longevity: Improving the durability and lifespan of sensors such as those based on PANI/N-doped graphene quantum dots (NGQDs) can reduce waste and lower the environmental footprint associated with sensor replacement. The NGQDs improved the structural stability and durability of PANI, contributing to SDG 9 by promoting innovation.

Optimize energy efficiency: Designing PANI-based sensors to operate at ultra-low power levels suitable for battery-powered and renewable energy-powered applications supports SDG 7. For example, the low-power operation of PANI/metal nanoparticle composites enables their use in remote or portable devices.

Integrate sensors with IoT for smart cities: Combining PANI-based chemiresistors with IoT technologies can create intelligent monitoring systems for urban environments. These systems support SDG 11 by enhancing urban resilience and environmental management through real-time air quality monitoring.

Support climate monitoring networks: Deploying PANI-based sensors in networks to monitor greenhouse gases and pollutants can provide critical data to inform climate policies and actions, aligning with SDG 13.

7. Conclusions

In this review, the underlying adverse problems related to exposure to harmful gases were introduced, and an emphasis on the importance of addressing these issues with advanced sensor technologies was presented. A range of gas sensors that are available in the market, such as catalytic gas sensors, electrochemical gas sensors, thermal conductivity gas sensors, optical gas sensors, non-dispersive infrared gas sensors, semiconductor gas sensors, surface acoustic wave sensors, gas chromatograph analyzers, film bulk acoustic resonators, photoionization detector gas sensors, and chemiresistor gas sensors were

discussed. Specifically, a discussion of the working principles of various gas-sensing technologies revealed a number of advantages and disadvantages associated with each sensing technology. These included detection accuracy, selectivity, operating temperature, stability over long periods and under different environments, cost of instrumentation for analysis, power consumption, response and recovery times, sensor installation costs, etc. A deeper look into various preparation methods for PANI composite materials revealed various innovation strategies that have been applied by various researchers in order to overcome the challenges associated with the use of PANI composites at room temperature. Strategies employed include the improvement of various parts of the gas sensor preparation steps such as optimization of composite structures, functionalization of PANI, incorporation of hybrid materials for synergistic effects, advanced fabrication technologies, etc. A further discussion of different types of PANI-based chemiresistive gas sensors, including PANI/polymer blends, PANI/carbon materials, PANI/metal nanoparticles, PANI/metal oxides, PANI/metal chalcogenides, and PANI/ternary composites was presented, accompanied by a discussion of the underlying sensing mechanisms. Based on the aforementioned, PANI composite materials were shown to exhibit substantial application potential in several areas, benefiting from miniaturized, simple, and efficient chemiresistor technology. Strategies for the future outlook of PANI-based chemiresistive gas sensors were also presented.

Author Contributions: Conceptualization, C.M.M. and E.C.L.-D.; writing—original draft preparation, data acquisition, methodology, C.M.M.; writing—review and editing, supervision E.C.L.-D., C.M.M., Z.T., L.Z.L., T.E.M. and N.M. All authors have read and agreed to the published version of the manuscript.

References

1. World Health Organization. *WHO Global Air Quality Guidelines: Particulate Matter (PM2.5 and PM10), Ozone, Nitrogen Dioxide, Sulfur Dioxide and Carbon Monoxide*; World Health Organization: Geneva, Switzerland, 2021. Available online: https://www.who.int/publications/i/item/9789240034228 (accessed on 8 July 2024).
2. David, E.; Niculescu, V.C. Volatile organic compounds (VOCs) as environmental pollutants: Occurrence and mitigation using nanomaterials. *Int. J. Environ. Res. Public Health* **2021**, *18*, 13147. [CrossRef] [PubMed]
3. Occupational Safety and Health Administration (OSHA). Toxic and Hazardous Substances. 29 CFR 1910 Subpart Z. Available online: https://www.osha.gov/laws-regs/regulations/standardnumber/1910/1910SubpartZ (accessed on 20 May 2024).
4. Dhall, S.; Mehta, B.R.; Tyagi, A.K.; Sood, K. A review on environmental gas sensors: Materials and technologies. *Sens. Int.* **2021**, *2*, 100116. [CrossRef]
5. Masemola, C.M.; Fadojutimi, P.; Maubane-Nkadimeng, M.; Tetana, Z.N.; Moloto, N.; Gqoba, S.; Linganiso, E.C. Ni$_3$S$_2$-HCSs Modified Polyaniline: Enhanced Ethanol Detection at Room Temperature. In Proceedings of the 2024 IEEE SENSORS, Kobe, Japan, 20–23 October 2024; pp. 1–4. [CrossRef]
6. Wen, J.; Wang, S.; Feng, J.; Ma, J.; Zhang, H.; Wu, P.; Li, G.; Wu, Z.; Meng, F.; Li, L.; et al. Recent progress in polyaniline-based chemiresistive flexible gas sensors: Design, nanostructures, and composite materials. *J. Mater. Chem. A* **2024**, *12*, 6190–6210. [CrossRef]

7. Karami, H.; Thurn, B.; de Boer, N.K.; Ramos, J.; Covington, J.A.; Lozano, J.; Liu, T.; Zhang, W.; Su, S.; Ueland, M. Application of gas sensor technology to locate victims in mass disasters–a review. *Nat. Hazards* **2024**, 1–30. [CrossRef]

8. Kalinin, I.A.; Roslyakov, I.V.; Bograchev, D.; Kushnir, S.E.; Ivanov, I.I.; Dyakov, A.V.; Napolskii, K.S. High performance microheater-based catalytic hydrogen sensors fabricated on porous anodic alumina substrates. *Sens. Actuators B Chem.* **2024**, *404*, 135270. [CrossRef]

9. Durani, F.; Mainuddin; Mittal, U.; Kumar, J.; Nimal, A.T. Use of surface acoustic wave (SAW) for thermal conductivity sensing of gases—A review. *IETE Tech. Rev.* **2021**, *38*, 611–621. [CrossRef]

10. Gardner, E.L.; Gardner, J.W.; Udrea, F. Micromachined thermal gas sensors—A review. *Sensors* **2023**, *23*, 681. [CrossRef] [PubMed]

11. Gardner, E.L.; De Luca, A.; Udrea, F. Differential Thermal Conductivity CO_2 Sensor. In Proceedings of the 2021 IEEE 34th International Conference on Micro Electro Mechanical Systems (MEMS), Gainesville, FL, USA, 25–29 January 2021; pp. 791–794. [CrossRef]

12. Barhoum, A.; Hamimed, S.; Slimi, H.; Othmani, A.; Abdel-Haleem, F.M.; Bechelany, M. Modern designs of electrochemical sensor platforms for environmental analyses: Principles, nanofabrication opportunities, and challenges. *Trends Environ. Anal. Chem.* **2023**, *38*, e00199. [CrossRef]

13. Hosseini, S.M.; Imanpour, A.; Rezavand, M.; Arjmandi Tash, A.M.; Antonini, S.; Rezvani, S.J.; Abdi, Y. Electrochemoresistance Sensor: A Borophene-Based Sensor with Simultaneous Electrochemical and Chemoresistance Sensing Capability. *ACS Mater. Lett.* **2024**, *6*, 933–942. [CrossRef]

14. Zhao, Y.; Liu, Y.; Han, B.; Wang, M.; Wang, Q.; Zhang, Y.N. Fiber optic volatile organic compound gas sensors: A review. *Coord. Chem. Rev.* **2023**, *493*, 215297. [CrossRef]

15. Liu, Y.; Zhang, Y.N.; Liu, S.; Shi, B.; Wang, L.; Zhao, Y. Fiber optic room temperature ethanol sensor based on $ZnSnO_3/TiO_2$ with UV radiation sensitization. *Sens. Actuators B Chem.* **2024**, *399*, 134814. [CrossRef]

16. Jha, R.K. Non-dispersive infrared gas sensing technology: A review. *IEEE Sens. J.* **2021**, *22*, 6–15. [CrossRef]

17. Yu, K.; Yang, X.; Wang, Y.; Zhang, P.; Zhang, L.; Tan, Q. A temperature-compensated CO2 detection system based on non-dispersive infrared spectral technology. *Rev. Sci. Instrum.* **2024**, *95*, 085002. [CrossRef]

18. Gao, L.; Tian, Y.; Hussain, A.; Guan, Y.; Xu, G. Recent developments and challenges in resistance-based hydrogen gas sensors based on metal oxide semiconductors. *Anal. Bioanal. Chem.* **2024**, *416*, 3697–3715. [CrossRef] [PubMed]

19. Yan, J.; Wang, Y.; Yang, C.; Deng, H.; Hu, N. MoS_2/MoO_3 heterojunctions enabled by surface oxidization of MoS_2 nanosheets for high-performance room-temperature NO_2 gas sensing. *J. Alloys Compd.* **2024**, *976*, 173208. [CrossRef]

20. Cui, B.; Ren, Z.; Wang, W.; Cheng, L.; Gao, X.; Huang, L.; Hu, A.; Hu, F.; Jin, J. Review of surface acoustic wave-based hydrogen sensor. *Sens. Actuators Rep.* **2024**, *7*, 100197. [CrossRef]

21. Tang, Z.; Wu, W.; Yang, P.; Luo, J.; Fu, C.; Han, J.C.; Zhou, Y.; Wang, L.; Wu, Y.; Huang, Y. A review of surface acoustic wave sensors: Mechanisms, stability and future prospects. *Sens. Rev.* **2024**, *44*, 249–266. [CrossRef]

22. Buiculescu, V.; Dinu, L.A.; Veca, L.M.; Pârvulescu, C.; Mihai, M.; Brîncoveanu, O.; Comănescu, F.; Brașoveanu, C.; Stoian, M.; Baracu, A.M. The development of sensitive graphene-based surface acoustic wave sensors for NO_2 detection at room temperature. *Microchim. Acta* **2024**, *191*, 323. [CrossRef]

23. Ren, J.; Chu, H.; Bai, Y.; Wang, R.; Chen, P.; Chen, J. Research and design of high sensitivity fbar micro-mass sensors. *IOP Conf. Ser. Earth Environ. Sci.* **2021**, *632*, 042014. [CrossRef]

24. Zhu, Y.; Xia, P.; Liu, J.; Fang, Z.; Du, L.; Zhao, Z. Polyimide-based high-performance film bulk acoustic resonator humidity sensor and its application in real-time human respiration monitoring. *Micromachines* **2022**, *13*, 758. [CrossRef]

25. Gao, C.; Fu, M.; Fan, S.; Ma, Z.; Tang, Y.; Hou, D.; Cao, Y. High-performance virtual sensors array based on a single-chip FBAR for volatile organic compounds (VOCs) detection and classification. *Sens. Actuators B Chem.* **2025**, *422*, 136687. [CrossRef]

26. Zimmer, C.M.; Kallis, K.T.; Giebel, F.J. Micro-structured electron accelerator for the mobile gas ionization sensor technology. *J. Sens. Sens. Syst.* **2015**, *4*, 151–157. [CrossRef]

27. Oliva, G.; Fiorillo, A.S.; Jelić, T.A.; Valić, S.; Pullano, S.A. Thermal desorption from zeolite layer for VOC detection. *Solid-State Electron.* **2023**, *210*, 108809. [CrossRef]

28. Prestage, J.; Day, C.; Husheer, S.L.; Winter, W.T.; Ho, W.O.; Saffell, J.R.; Hutter, T. Selective detection of volatile organics in a mixture using a photoionization detector and thermal desorption from a nanoporous preconcentrator. *ACS Sens.* **2021**, *7*, 304–311. [CrossRef] [PubMed]

29. Al-Bukhaiti, W.Q.; Noman, A.; Qasim, A.S.; Al-Farga, A. Gas chromatography: Principles, advantages and applications in food analysis. *Int. J. Agric. Innov. Res.* **2017**, *6*, 123–128. Available online: https://www.researchgate.net/profile/Ammar_Al-Farga/publication/342360886_Gas_Chromatography_Principles_Advantages_and_Applications_in_Food_Analysis/links/5f1a26c8299bf1720d5fc2e3/Gas-Chromatography-Principles-Advantages-and-Applications-in-Food-Analysis.pdf?origin=journalDetail&_tp=eyJwYWdlIjoiam91cm5hbERldGFpbCJ9 (accessed on 8 January 2025).

30. Aghili, N.S.; Rasekh, M.; Karami, H.; Edriss, O.; Wilson, A.D.; Ramos, J. Aromatic fingerprints: VOC analysis with E-nose and GC-MS for rapid detection of adulteration in sesame oil. *Sensors* **2023**, *23*, 6294. [CrossRef] [PubMed]

31. Zhang, L.; Tian, J.; Wang, Y.; Wang, T.; Wei, M.; Li, F.; Li, D.; Yang, Y.; Yu, H.; Dong, X. Polyoxometalates electron acceptor-intercalated In_2O_3@SnO_2 nanofibers for chemiresistive ethanol gas sensors. *Sens. Actuators B Chem.* **2024**, *410*, 135728. [CrossRef]

32. Najafi, P.; Ghaemi, A. Chemiresistor gas sensors: Design, Challenges, and Strategies: A comprehensive review. *Chem. Eng. J.* **2024**, *498*, 154999. [CrossRef]

33. Kumar, A.; Mirzaei, A.; Lee, M.H.; Ghahremani, Z.; Kim, T.U.; Kim, J.Y.; Kwoka, M.; Kumar, M.; Kim, S.S.; Kim, H.W. Strategic review of gas sensing enhancement ways of 2D tungsten disulfide/selenide based chemiresistive sensors: Decoration and composite. *J. Mater. Chem. A* **2024**, *12*, 3771–3806. [CrossRef]

34. Wang, P.; Tang, C.; Song, H.; Zhang, L.; Lu, Y.; Huang, F. 1D/2D Heterostructured WS2@ PANI Composite for Highly Sensitive, Flexible, and Room Temperature Ammonia Gas Sensor. *ACS Appl. Mater. Interfaces* **2024**, *16*, 14082–14092. [CrossRef] [PubMed]

35. Sharma, A.; Eadi, S.B.; Noothalapati, H.; Otyepka, M.; Lee, H.D.; Jayaramulu, K. Porous materials as effective chemiresistive gas sensors. *Chem. Soc. Rev.* **2024**, *53*, 2530–2577. [CrossRef] [PubMed]

36. Boublia, A.; Guezzout, Z.; Haddaoui, N.; Badawi, M.; Darwish, A.S.; Lemaoui, T.; Lebouachera, S.E.I.; Yadav, K.K.; Alreshidi, M.A.; Algethami, J.S.; et al. The curious case of polyaniline-graphene nanocomposites: A review on their application as exceptionally conductive and gas sensitive materials. *Crit. Rev. Solid State Mater. Sci.* **2023**, *49*, 973–997. [CrossRef]

37. Ali, Z.S.; Shano, A.M. The influence of solvents on polyaniline nanofibers synthesized by a hydrothermal method and their application in gas sensors. *J. Electron. Mater.* **2020**, *49*, 5528–5533. [CrossRef]

38. Samotaev, N.; Podlepetsky, B.; Mashinin, M.; Ivanov, I.; Obraztsov, I.; Oblov, K.; Dzhumaev, P. Thermal Conductivity Gas Sensors for High-Temperature Applications. *Micromachines* **2024**, *15*, 138. [CrossRef] [PubMed]

39. Wu, J.; Yue, G.; Chen, W.; Xing, Z.; Wang, J.; Wong, W.R.; Cheng, Z.; Set, S.Y.; Senthil Murugan, G.; Wang, X.; et al. On-chip optical gas sensors based on group-IV materials. *ACS Photonics* **2020**, *7*, 2923–2940. [CrossRef]

40. Liang, J.G.; Jiang, Y.; Wu, J.K.; Wang, C.; von Gratowski, S.; Gu, X.; Pan, L. Multiplex-gas detection based on non-dispersive infrared technique: A review. *Sens. Actuators A Phys.* **2023**, 114318. [CrossRef]

41. Goel, N.; Kunal, K.; Kushwaha, A.; Kumar, M. Metal oxide semiconductors for gas sensing. *Eng. Rep.* **2023**, *5*, e12604. [CrossRef]

42. Aslam, M.Z.; Zhang, H.; Sreejith, V.S.; Naghdi, M.; Ju, S. Advances in the surface acoustic wave sensors for industrial applications: Potentials, challenges, and future directions: A review. *Measurement* **2023**, *222*, 113657. [CrossRef]

43. Patel, R.; Adhikari, M.S.; Tripathi, S.K.; Sahu, S. Design, optimization and performance assessment of single port film bulk acoustic resonator through finite element simulation. *Sensors* **2023**, *23*, 8920. [CrossRef]

44. Galvani, M.; Freddi, S.; Sangaletti, L. Disclosing Fast Detection Opportunities with Nanostructured Chemiresistor Gas Sensors Based on Metal Oxides, Carbon, and Transition Metal Dichalcogenides. *Sensors* **2024**, *24*, 584. [CrossRef] [PubMed]

45. Su, P.; Li, W.; Zhang, J.; Xie, X. Chemiresistive gas sensor based on electrospun hollow SnO_2 nanotubes for detecting NO at the ppb level. *Vacuum* **2022**, *199*, 110961. [CrossRef]

46. Chiang, C.K.; Fincher, C.R., Jr.; Park, Y.W.; Heeger, A.J.; Shirakawa, H.; Louis, E.J.; Gau, S.C.; MacDiarmid, A.G. Electrical conductivity in doped polyacetylene. *Phys. Rev. Lett.* **1977**, *39*, 1098. [CrossRef]

47. Heeger, A.J.; MacDiarmid, A.G.; Shirakawa, H. The Nobel Prize in chemistry, 2000: Conductive polymers. *R. Swed. Acad. Sci.* **2000**, 1–16. Available online: https://www.nobelprize.org/prizes/chemistry/2000/summary/ (accessed on 8 January 2025).

48. Verma, A.; Gupta, R.; Verma, A.S.; Kumar, T. A review of composite conducting polymer-based sensors for detection of industrial waste gases. *Sens. Actuators Rep.* **2023**, *5*, 100143. [CrossRef]

49. Li, B.; Li, Y.; Ma, P. Synthesis of different inorganic acids doped polyaniline materials and behavior of enhancing NH_3 gas sensing properties. *Org. Electron.* **2023**, *114*, 106749. [CrossRef]

50. Dimple; Madan, R.; Kumar, V.; Mohan, D.; Garg, R. Acetone gas sensing behavior of polypyrrole/ZnO nanocomposites synthesized via chemical oxidation method. *J. Mater. Sci. Mater. Electron.* **2024**, *35*, 130. [CrossRef]

51. Gopika, R.; Arun, K.; Ramesan, M.T. In-situ polymerization of polythiophene/silicon carbide nanocomposites for gas sensing and optoelectronic devices. *J. Mater. Res. Technol.* **2024**, *30*, 1288–1300. [CrossRef]

52. Gu, Y.; Liu, L.; Wang, Y.; Zhang, C.; Satoh, T. Chromaticity sensor for discriminatory identification of aliphatic and aromatic primary amines based on conformational changes of polyacetylene. *Talanta* **2024**, *268*, 125361. [CrossRef] [PubMed]

53. Wong, Y.C.; Ang, B.C.; Haseeb, A.S.M.A.; Baharuddin, A.A.; Wong, Y.H. Conducting polymers as chemiresistive gas sensing materials: A review. *J. Electrochem. Soc.* **2020**, *167*, 037503. [CrossRef]

54. Joke, O.F.; Rotimi, I.A.; Makhatha, M.E.; Olaoye, O.P.; Yetunde, S.A.; Joy, O.O.; Victoria, O.T.; Bayode, A.T.; Ayantunde, A.A. Investigation of the Gas Sensing Potential of Electrospun Expanded Polystyrene/Reduced Graphene Oxide Nanofiber Composites. In *Chemical and Materials Sciences—Developments and Innovations*; BP International: Hong Kong, China, 2024. [CrossRef]

55. Rath, R.J.; Farajikhah, S.; Oveissi, F.; Shahrbabaki, Z.; Yun, J.; Naficy, S.; Dehghani, F. A Polymer-Based Chemiresistive Gas Sensor for Selective Detection of Ammonia Gas. *Adv. Sens. Res.* **2024**, *3*, 2300125. [CrossRef]

56. Guo, X.; Sun, Y.; Sun, X.; Li, J.; Wu, J.; Shi, Y.; Pan, L. Doping engineering of conductive polymers and their application in physical sensors for healthcare monitoring. *Macromol. Rapid Commun.* **2024**, *45*, 2300246. [CrossRef]

57. Hashemi Karouei, S.F.; Milani Moghaddam, H.; Saadat Niavol, S. Characterization and gas sensing sproperties of graphene/polyaniline nanocomposite with long-term stability under high humidity. *J. Mater. Sci.* **2021**, *56*, 4239–4253. [CrossRef]

58. Le, C.V.; Yoon, H. Advances in the Use of Conducting Polymers for Healthcare Monitoring. *Int. J. Mol. Sci.* **2024**, *25*, 1564. [CrossRef]

59. Rodrigues, J.; Jain, S.; Shimpi, N.G. Conducting polymer-based gas sensors. In *Carbon-Based Nanomaterials and Nanocomposites for Gas Sensing*; Elsevier: Amsterdam, The Netherlands, 2023; pp. 181–232. [CrossRef]

60. Lawaniya, S.D.; Kumar, S.; Yu, Y.; Awasthi, K. Ammonia sensing properties of PPy nanostructures (urchins/flowers) towards low-cost and flexible gas sensors at room temperature. *Sens. Actuators B Chem.* **2023**, *382*, 133566. [CrossRef]

61. Ding, H.; Hussein, A.M.; Ahmad, I.; Latef, R.; Abbas, J.K.; Abd Ali, A.T.; Saeed, S.M.; Abdulwahid, A.S.; Ramadan, M.F.; Rasool, H.A.; et al. Conducting polymers in industry: A comprehensive review on the characterization, synthesis and application. *Alex. Eng. J.* **2024**, *88*, 253–267. [CrossRef]

62. Jang, H.J.; Shin, B.J.; Jung, E.Y.; Bae, G.T.; Kim, J.Y.; Tae, H.S. Polypyrrole film synthesis via solution plasma polymerization of liquid pyrrole. *Appl. Surf. Sci.* **2023**, *608*, 155129. [CrossRef]

63. Nadekar, B.; Gund, G.S.; Khollam, Y.B.; Shaikh, S.F.; Wavhal, D.S.; Dubal, D.P.; More, P. Plasma-polymerized and iodine-doped polyvinyl acetate for volatile organic compound gas sensing applications. *ACS Appl. Polym. Mater.* **2023**, *5*, 1882–1890. [CrossRef]

64. Pavel, I.A.; Lasserre, A.; Simon, L.; Rossignol, J.; Lakard, S.; Stuerga, D.; Lakard, B. Microwave Gas Sensors Based on Electrode-posited Polypyrrole–Nickel Phthalocyanine Hybrid Films. *Sensors* **2023**, *23*, 5550. [CrossRef] [PubMed]

65. Sharma, A.; Rawal, I.; Rajpal, A.; Khokhar, A.; Kumar, V.; Goyal, P.K. Highly sensitive and selective room temperature ammonia sensor based on polyaniline thin film: In situ dip-coating polymerization. *J. Mater. Sci. Mater. Electron.* **2022**, *33*, 14071–14085. [CrossRef]

66. Bibi, A.; Rubio, Y.R.M.; Santiago, K.S.; Jia, H.W.; Ahmed, M.M.; Lin, Y.F.; Yeh, J.M. H_2S-sensing studies using interdigitated electrode with spin-coated carbon aerogel-polyaniline composites. *Polymers* **2021**, *13*, 1457. [CrossRef] [PubMed]

67. Gu, W.; Li, Q.; Wang, R.; Zhang, L.; Liu, Z.; Jiao, T. Recent Progress in the Applications of Langmuir–Blodgett Film Technology. *Nanomaterials* **2024**, *14*, 1039. [CrossRef] [PubMed]

68. Abdulla, S.; Pullithadathil, B. Unidirectional Langmuir–Blodgett-mediated alignment of polyaniline-functionalized multiwalled carbon nanotubes for NH_3 gas sensor applications. *Langmuir* **2020**, *36*, 11618–11628. [CrossRef] [PubMed]

69. Tan, H.; Chu, Y.; Wu, X.; Liu, W.J.; Zhang, D.W.; Ding, S.J. High-performance flexible gas sensors based on layer-by-layer assembled polythiophene thin films. *Chem. Mater.* **2021**, *33*, 7785–7794. [CrossRef]

70. Majumdar, S.; Sarmah, K.; Mahanta, D. A simple route to prepare polypyrrole-coated filter papers via vapor phase polymerization and their gas sensing application. *ACS Appl. Polym. Mater.* **2020**, *2*, 1933–1942. [CrossRef]

71. Matsuguchi, M.; Nakamae, T.; Fujisada, R.; Shiba, S. A highly sensitive ammonia gas sensor using Micrometer-Sized Core–Shell-Type spherical polyaniline particles. *Sensors* **2021**, *21*, 7522. [CrossRef]

72. Han, K.H.; Kang, H.; Lee, G.Y.; Lee, H.J.; Jin, H.M.; Cha, S.K.; Yun, T.; Kim, J.H.; Yang, G.G.; Choi, H.J.; et al. Highly aligned carbon nanowire array by e-field directed assembly of PAN-containing block copolymers. *ACS Appl. Mater. Interfaces* **2020**, *12*, 58113–58121. [CrossRef] [PubMed]

73. Wang, S.; Li, H.; Huang, H.; Cao, X.; Chen, X.; Cao, D. Porous organic polymers as a platform for sensing applications. *Chem. Soc. Rev.* **2022**, *51*, 2031–2080. [CrossRef]

74. Shakeel, A.; Rizwan, K.; Farooq, U.; Iqbal, S.; Altaf, A.A. Advanced polymeric/inorganic nanohybrids: An integrated platform for gas sensing applications. *Chemosphere* **2022**, *294*, 133772. [CrossRef] [PubMed]

75. Keerthana, M.; Suma, M.S.; Jisha, P.; Vinjamuri, S.; Vijayalakshmi, K. Analysis of Structural, Morphological and Optical Characteristics of Protonic Acids Doped Polyaniline For VOC Sensing Application. In Proceedings of the 2024 International Conference on Smart Systems for applications in Electrical Sciences (ICSSES), Tumakuru, India, 3–4 May 2024; pp. 1–6. [CrossRef]

76. Duan, X.; Duan, Z.; Zhang, Y.; Liu, B.; Li, X.; Zhao, Q.; Yuan, Z.; Jiang, Y.; Tai, H. Enhanced NH_3 sensing performance of polyaniline via a facile morphology modification strategy. *Sens. Actuators B Chem.* **2022**, *369*, 132302. [CrossRef]

77. Singh, P.; Shukla, S.K. Advances in polyaniline-based nanocomposites. *J. Mater. Sci.* **2020**, *55*, 1331–1365. [CrossRef]

78. Li, B.; Li, Y.; Ma, P. The effect of different protonic acid doping on the sensitivity of polyaniline to ammonia gas. *J. Mater. Sci. Mater. Electron.* **2024**, *35*, 401. [CrossRef]

79. Lv, D.; Shen, W.; Chen, W.; Tan, R.; Xu, L.; Song, W. PSS-PANI/PVDF composite based flexible NH3 sensors with sub-ppm detection at room temperature. *Sens. Actuators B Chem.* **2021**, *328*, 129085. [CrossRef]

80. Devi, L.S.; Daniel, T.T.; Paily, R.; Dasmahapatra, A.K. Polyaniline/Poly (vinyl alcohol) Conductive Hydrogel for a Chemiresistive Ultrasensitive Ammonia Gas Sensor. *ACS Appl. Polym. Materials.* **2024**, *6*, 10603–10614. [CrossRef]

81. Kayishaer, A.; Duc, C.; Magnenet, C.; Lakard, B.; Halima, H.B.; Redon, N.; Lakard, S. Fluorinated polyaniline-based sensors with enhanced NH3 sensitivity. *Synth. Met.* **2024**, *307*, 117695. [CrossRef]

82. Chaudhary, V. Charge carrier dynamics of electrochemically synthesized poly (aniline co-pyrrole) nanospheres based sulfur dioxide chemiresistor. *Polym.-Plast. Technol. Mater.* **2022**, *61*, 107–115. [CrossRef]

83. Li, P.; Xu, H.; Liu, F.; Shi, J.; Gao, X.; Li, J. Room-temperature NH_3 sensors based on polyaniline-assembled graphitic carbon nitride nanosheets. *ACS Appl. Nano Mater.* **2023**, *6*, 5145–5154. [CrossRef]

84. Masemola, C.M.; Moloto, N.; Tetana, Z.N.; Gqoba, S.S.; Mubiayi, P.K.; Linganiso, E.C. N-doped graphene quantum dot-modified polyaniline for room-temperature sensing of alcohol vapors. *Mater. Chem. Phys.* **2022**, *287*, 126229. [CrossRef]

85. Chen, X.; Xing, X.; Li, Z.; Zhao, X.; Tian, Y.; Lang, X.; Yang, D. Three-dimensional porous carbon framework coated with polyaniline for highly stable and selective ammonia sensing. *Sens. Actuators B Chem.* **2023**, *395*, 134539. [CrossRef]

86. Singh, R.; Agrohiya, S.; Rawal, I.; Ohlan, A.; Dahiya, S.; Punia, R.; Maan, A.S. Multifunctional porous polyaniline/phosphorus-nitrogen co-doped graphene nanocomposite for efficient room temperature ammonia sensing and high-performance supercapacitor applications. *Appl. Surf. Sci.* **2024**, *665*, 160368. [CrossRef]

87. Xiao, G.; Weng, H.; Ge, L.; Huang, Q. Application status of carbon nanotubes in fire detection sensors. *Front. Mater.* **2020**, *7*, 588521. [CrossRef]

88. Amarnath, M.; Gurunathan, K. Highly selective CO_2 gas sensor using stabilized NiO-In_2O_3 nanospheres coated reduced graphene oxide sensing electrodes at room temperature. *J. Alloys Compd.* **2021**, *857*, 157584. [CrossRef]

89. Adhav, P.; Pawar, D.; Diwate, B.; Bora, M.; Jagtap, S.; Chourasia, A.; Dallavalle, S.; Chabukswar, V. Room temperature operable ultra-sensitive ammonia sensor based on polyaniline-silver (PANI-Ag) nanocomposites synthesized by ultra-sonication. *Synth. Met.* **2023**, *293*, 117237. [CrossRef]

90. Verma, A.; Kumar, T. Ag/Cu doped polyaniline hybrid nanocomposite-based novel gas sensor for enhanced ammonia gas sensing performance at room temperature. *RSC Adv.* **2024**, *14*, 25093–25107. [CrossRef] [PubMed]

91. Verma, A.; Kumar, T. Gas sensing properties of a Cu-doped PANI nanocomposite towards ammonia. *Mater. Adv.* **2024**, *5*, 7387–7400. [CrossRef]

92. Kulkarni, S.B.; Navale, Y.H.; Navale, S.T.; Stadler, F.J.; Patil, V.B. Room temperature ammonia gas sensing properties of polyaniline nanofibers. *J. Mater. Sci. Mater. Electron.* **2019**, *30*, 8371–8380. [CrossRef]

93. Qu, Y.; Zheng, H.; Lei, Y.; Ding, Z.; Li, S.; Liu, S.; Ji, W. Room Temperature NH_3 Selective Gas Sensors Based on Double-Shell Hierarchical $SnO_2@$ polyaniline Composites. *Sensors* **2024**, *24*, 1824. [CrossRef]

94. Dhanawade, R.N.; Pawar, N.S.; Chougule, M.A.; Hingangavkar, G.M.; Jadhav, Y.M.; Nimbalkar, T.M.; Navale, Y.H.; Chavan, G.T.; Jeon, C.W.; Patil, V.B. Highly sensitive and selective PAni-CeO_2 nanohybrid for detection of NH3 biomarker at room temperature. *J. Mater. Sci. Mater. Electron.* **2023**, *34*, 781. [CrossRef]

95. Zhang, B.; Shang, F.; Shi, X.; Yao, R.; Wei, F.; Hou, X.; Li, W.; Zhang, J. Polyaniline/CuO nanoparticle composites for use in selective H2S sensors. *ACS Appl. Nano Mater.* **2023**, *6*, 18413–18425. [CrossRef]

96. Saravanan, K.K.; Siva Karthik, P.; Mirtha, P.R.; Balaji, J.; Rajeshkanna, B. A one-pothydrothermal-induced PANI/SnO_2 and PANI/SnO_2/rGO ternary composites for high-performance chemiresistive-based H_2S and NH_3 gas sensors. *J. Mater. Sci. Mater. Electron.* **2020**, *31*, 8825–8836. [CrossRef]

97. Kaur, R.; Lawaniya, S.D.; Kumar, S.; Saini, N.; Awasthi, K. Nanoarchitectonics of polyaniline–zinc oxide (PANI–ZnO) nanocomposite for enhanced room temperature ammonia sensing. *Appl. Phys. A* **2023**, *129*, 765. [CrossRef]

98. Pal, R.; Goyal, S.L.; Rawal, I. Selective methanol sensors based on polyaniline/V_2O_5 nanocomposites. *Iran. Polym. J.* **2022**, *31*, 519–532. [CrossRef]

99. Fadojutimi, P.; Masemola, C.; Maubane-Nkadimeng, M.; Linganiso, E.; Tetana, Z.; Moma, J.; Moloto, N.; Gqoba, S. Room temperature sensing of primary alcohols via polyaniline/zirconium disulphide. *Heliyon* **2023**, *9*, e16216. [CrossRef]

100. Feng, Z.; Wen, J.; Meng, F.; Tian, R.; Wang, S.; Wang, K.; Tian, Y. In Situ-Polymerized PANI/WS2 Nanocomposites for Highly Sensitive Flexible Ammonia Gas Sensors and Respiration Monitoring Devices. *ACS Appl. Nano Mater.* **2024**, *7*, 3385–3393. [CrossRef]

101. Chen, X.; Chen, X.; Ding, X.; Yu, X. Gas Sensitive Characteristics of Polyaniline Decorated with Molybdenum Ditelluride Nanosheets. *Chemosensors* **2022**, *10*, 264. [CrossRef]

102. Ghaleghafi, E.; Rahmani, M.B. Reversible room temperature ammonia sensor based on the synthesized MoS_2/PANI nanocomposites. *Phys. Scr.* **2023**, *98*, 075801. [CrossRef]

103. Upadhye, D.S.; Dive, A.S.; Birajadar, R.B.; Bagul, S.B.; Gattu, K.P.; Sharma, R. Low-concentration ammonia gas sensing using polyaniline nanofiber thin film grown by rapid polymerization technique. *J. Mater. Sci. Mater. Electron.* **2022**, *33*, 23016–23029. [CrossRef]

104. Qiu, C.; Zhang, H.; Li, Q.; Guo, Y.; Song, Y.; An, F.; Zhu, L.; Xiao, A.; Lv, C.; Zhang, D. PANI/$CoMoO_4$ Nanocomposite Heterostructures for Detection of NH3 at Room Temperature. *ACS Appl. Nano Mater.* **2023**, *7*, 857–865. [CrossRef]

105. Masemola, C.M.; Shumbula, N.P.; Gqoba, S.S.; Tetana, Z.N.; Moloto, N.; Linganiso, E.C. Electrospun NGQDs/PANI/PAN composite fibers for room temperature alcohol sensing. In Proceedings of the 2021 IEEE 3rd Eurasia Conference on IOT, Communication and Engineering (ECICE), Yunlin, Taiwan, 29–31 October 2021; pp. 146–150. [CrossRef]

106. Rahim, M.; Ullah, R.; Ahmad, N.; Rahim, I.; Yaseen, S. Synthesis and characterization of highly sensitive ammonia sensor based on polyaniline/bismuth doped zinc oxide composites. *Polym. Compos.* **2024**, *45*, 10418–10429. [CrossRef]

107. Mathe, B.N.; Masemola, C.M.; Moma, J.; Tetana, Z.N.; Linganiso, E.C. Room temperature ammonia gas sensing using polyaniline/indium oxide/onion-like carbon composite. In Proceedings of the 2023 IEEE SENSORS, Vienna, Austria, 29 October–1 November 2023; pp. 1–4. [CrossRef]

108. Hadano, F.S.; Gavim, A.E.X.; Stefanelo, J.C.; Gusso, S.L.; Macedo, A.G.; Rodrigues, P.C.; Mohd Yusoff, A.R.B.; Schneider, F.K.; Deus, J.F.D.; José da Silva, W. NH$_3$ sensor based on rGO-PANI composite with improved sensitivity. *Sensors* **2021**, *21*, 4947. [CrossRef] [PubMed]

109. Mekki, A.; Joshi, N.; Singh, A.; Salmi, Z.; Jha, P.; Decorse, P.; Lau-Truong, S.; Mahmoud, R.; Chehimi, M.M.; Aswal, D.K.; et al. H$_2$S sensing using in situ photo-polymerized polyaniline–silver nanocomposite films on flexible substrates. *Org. Electron.* **2014**, *15*, 71–81. [CrossRef]

110. Gautam, S.K.; Panda, S. Highly sensitive Cu-ethylenediamine/PANI composite sensor for NH$_3$ detection at room temperature. *Talanta* **2023**, *258*, 124418. [CrossRef]

111. Wang, P.; Tang, C.; Zhang, L.; Lu, Y.; Huang, F. Hierarchical 0D/1D/2D Au/PANI/WS2 ternary nanocomposite NH$_3$ sensor with high performance and fast response/recovery for food spoilage detection. *Chem. Eng. J.* **2024**, *496*, 153998. [CrossRef]

112. Pegu, B.; Konwar, M.; Sarma, D.; Konwer, S. Cu nanoparticle anchored highly conducting, reusable multifunctional rGO/PANI nanocomposite: A novel material for methanol sensor and a catalyst for click reaction. *Synth. Met.* **2024**, *301*, 117516. [CrossRef]

113. Benhouhou, S.; Mekki, A.; Ayat, M.; Gabouze, N. Facile Preparation of PANI-Sr Composite Flexible Thin Film for Ammonia Sensing at Very Low Concentration. *Macromol. Res.* **2021**, *29*, 267–279. [CrossRef]

114. Chen, G.; Yuan, Y.; Zhang, H.; Lang, M.; Cheng, Y. Design of high-performance ternary ammonia gas sensors based on Au NPs hybrid PANI-TiO2 nanocomposites on flexible polyimide substrate. In Proceedings of the 10th International Symposium on Advanced Optical Manufacturing and Testing Technologies: Intelligent Sensing Technologies and Applications, Chengdu, China, 14–17 June 2021; Volume 12075, pp. 90–103. [CrossRef]

115. Wu, Q.; Shen, W.; Lv, D.; Chen, W.; Song, W.; Tan, R. An enhanced flexible room temperature ammonia gas sensor based on GP-PANI/PVDF multi-hierarchical nanocomposite film. *Sens. Actuators B Chem.* **2021**, *334*, 129630. [CrossRef]

116. Thangamani, G.J.; Deshmukh, K.; Nambiraj, N.A.; Pasha, S.K. Chemiresistive gas sensors based on vanadium pentoxide reinforced polyvinyl alcohol/polypyrrole blend nanocomposites for room temperature LPG sensing. *Synth. Met.* **2021**, *273*, 116687. [CrossRef]

117. Mohammed, H.Y.; Birare, M.S.; Farea, M.A.; Murshed, M.N.; El Sayed, M.E.; Samir, A.; Dole, B.N.; Shirsat, M.D. Accelerated kinetics for room temperature carbon monoxide sensing enabled by silver chloride-modified protonated polyaniline/graphene oxide. *Appl. Phys. A* **2024**, *130*, 39. [CrossRef]

118. Kumar, M.; Sharma, S.; Pal, R.; Vidhani, B. A novel gas sensor based on activated charcoal and polyaniline composites for selective sensing of methanol vapors. *Sens. Actuators A Phys.* **2023**, *353*, 114210. [CrossRef]

119. Selvakumar, D.; Sonu, K.P.; Ramadoss, G.; Sivaramakrishnan, R.; Jayavel, R.; Eswaramoorthy, M.; Rao, K.V.; Pugazhendhi, A. Heterostructures of polyaniline and Ce–ZnO nanomaterial coated flexible PET thin films for LPG gas sensing at standard environment. *Chemosphere* **2023**, *314*, 137492. [CrossRef] [PubMed]

120. Akbar, A.; Das, M.; Sarkar, D. Room temperature ammonia sensing by CdS nanoparticle decorated polyaniline (PANI) nanorods. *Sens. Actuators A Phys.* **2020**, *310*, 112071. [CrossRef]

121. Tian, X.; Cui, X.; Xiao, Y.; Chen, T.; Xiao, X.; Wang, Y. Pt/MoS$_2$/polyaniline nanocomposite as a highly effective room temperature flexible gas sensor for ammonia detection. *ACS Appl. Mater. Interfaces* **2023**, *15*, 9604–9617. [CrossRef] [PubMed]

122. Karmakar, N.; Jain, S.; Fernandes, R.; Shah, A.; Patil, U.; Shimpi, N.; Kothari, D. Enhanced sensing performance of an ammonia gas sensor based on Ag-decorated ZnO nanorods/polyaniline nanocomposite. *ChemistrySelect* **2023**, *8*, e202204284. [CrossRef]

123. Rezaei, B.; Gholami, E.; Taromi, F.A.; Haghighi, A.H. In situ synthesis of long tubular water-dispersible polyaniline with core/shell gold and silver@ graphene oxide nanoparticles for gas sensor application. *Heliyon* **2024**, *10*, e26662. [CrossRef]

124. Lee, J.H.; Kim, J.Y.; Mirzaei, A.; Nam, M.S.; Kim, H.W.; Kim, S.S. Room-temperature detection of acetone gas by PANI/NiO-loaded TiO$_2$ nanoparticles under UV irradiation. *Sens. Actuators B Chem.* **2023**, *374*, 132850. [CrossRef]

125. Li, P.; Li, J.; Liu, F.; Shi, J.; Gao, X.; Xu, H. Cu-Loaded Polyaniline-Coated MoO$_3$ Nanowire Nanohybrids for High-Sensitivity NH3 Sensing at Room Temperature. *ACS Appl. Nano Mater.* **2023**, *6*, 17423–17432. [CrossRef]

126. Yu, Y.H.; Lin, X.Y.; Teng, K.L.; Hu, C.C.; Wang, W.Y.; Hung, Y.H.; Tseng, H.Y.; Luo, K.H.; Yeh, J.M.; Lu, K.L.; et al. Semiconductive (Cu–S) n Metal–Organic Frameworks Hybrid Polyaniline Nanocomposites as Hydrogen Sulfide Gas Sensor. *Surf. Interfaces* **2024**, *44*, 103698. [CrossRef]

127. Ali, Z.M.; Murshed, M.N.; El Sayed, M.E.; Samir, A.; Alsharabi, R.M.; Farea, M.O. A new fabrication strategy of Ag_2O doped PANI as a highly stable and room temperature operable carbon monoxide gas sensor. *Opt. Mater.* **2023**, *144*, 114324. [CrossRef]

128. Luo, M.; Xiong, D.; Huang, X.; Cai, S.; Li, S.; Jia, Z.; Gao, Z. V2CTx@PANI Nanocomposite as a Highly Effective Room Temperature Gas Sensor for Ammonia Detection. *J. Alloys Compd.* **2024**, 176340. [CrossRef]

129. Tang, B.; Shi, Y.; Liu, J.; Zheng, C.; Zhao, K.; Zhang, J.; Feng, Q. Low-Drift NO_2 Sensor Based on Polyaniline/Black Phosphorus Composites at Room Temperature. *Chemosensors* **2024**, *12*, 181. [CrossRef]